

Fundamental limits on the rate of bacterial cell division

³ **Nathan M. Belliveau^{†, 1}, Griffin Chure^{†, 2, 3}, Christina L. Hueschen⁴, Hernan G.
⁴ Garcia⁵, Jané Kondev⁶, Daniel S. Fisher⁷, Julie Theriot^{1, 8}, Rob Phillips^{2, 9, *}**

*For correspondence:

[†]These authors contributed equally to this work

⁵ ¹Department of Biology, University of Washington, Seattle, WA, USA; ²Division of
⁶ Biology and Biological Engineering, California Institute of Technology, Pasadena, CA,
⁷ USA; ³Department of Applied Physics, California Institute of Technology, Pasadena, CA,
⁸ USA; ⁴Department of Chemical Engineering, Stanford University, Stanford, CA, USA;
⁹ ⁵Department of Molecular Cell Biology and Department of Physics, University of
¹⁰ California Berkeley, Berkeley, CA, USA; ⁶Department of Physics, Brandeis University,
¹¹ Waltham, MA, USA; ⁷Department of Applied Physics, Stanford University, Stanford, CA,
¹² USA; ⁸Allen Institute for Cell Science, Seattle, WA, USA; ⁹Department of Physics,
¹³ California Institute of Technology, Pasadena, CA, USA; *Contributed equally

¹⁴

¹⁵ **Abstract** This will be written next (promise).

¹⁶

¹⁷ Introduction

¹⁸ The range of bacterial growth rates is enormously diverse. In natural environments, some micro-
¹⁹ bial organisms might double only once per year while in comfortable laboratory conditions, growth
²⁰ can be rapid with several divisions per hour. This six order of magnitude difference illustrates the
²¹ intimate relationship between environmental conditions and the rates at which cells convert nu-
²² trients into new cellular material – a relationship that has remained a major topic of inquiry in
²³ bacterial physiology for over a century (*Jun et al., 2018*). As was noted by Jacques Monod, “the
²⁴ study of the growth of bacterial cultures does not constitute a specialized subject or branch of re-
²⁵ search, it is the basic method of Microbiology.” Those words ring as true today as they did when
²⁶ they were written 70 years ago. Indeed, the study of bacterial growth has undergone a molecular
²⁷ resurgence since many of the key questions addressed by the pioneering efforts in the middle of
²⁸ the last century can be revisited by examining them through the lens of the increasingly refined
²⁹ molecular census that is available for bacteria such as the microbial workhorse *Escherichia coli*. Sev-
³⁰ eral of the outstanding questions that can now be studied about bacterial growth include: what
³¹ sets the fastest time scale that bacteria can divide, and how is growth rate tied to the quality of the
³² carbon source. In this paper, we address these two questions from two distinct angles. First, as
³³ a result of an array of high-quality proteome-wide measurements of the *E. coli* proteome under a
³⁴ myriad of different growth conditions, we have a census that allows us to explore how the num-
³⁵ ber of key molecular players change as a function of growth rate. This census provides a window
³⁶ onto whether the processes they mediate such as molecular transport into the cells and molecular
³⁷ synthesis within cells can run faster. Second, because of our understanding of the molecular path-
³⁸ ways responsible for many of the steps in bacterial growth, we can also make order of magnitude
³⁹ estimates to infer the copy numbers that would be needed to achieve a given growth rate. In this
⁴⁰ paper, we pass back and forth between the analysis of a variety of different proteomic datasets and
⁴¹ order-of-magnitude estimations to determine possible molecular bottlenecks that limit bacterial

42 growth and to see how the growth rate varies in different carbon sources.

43 Specifically, we leverage a combination of *E. coli* proteomic data sets collected over the past
 44 decade using either mass spectrometry (*Schmidt et al., 2016; Peebo et al., 2015; Valgepea et al.,
 45 2013*) or ribosomal profiling (*Li et al., 2014*) across 31 unique growth conditions. Broadly speaking,
 46 we entertain several classes of hypotheses as are illustrated in **Figure 1**. First, we consider potential
 47 limits on the transport of nutrients into the cell. We address this hypothesis by performing an
 48 order-of-magnitude estimate for how many carbon, phosphorous, and sulfur atoms are needed to
 49 facilitate this requirement given a 5000 second division time. As a second hypothesis, we consider
 50 the possibility that there exists a fundamental limit on how quickly the cell can generate ATP. We
 51 approach this hypothesis from two angles, considering how many ATP synthase complexes must
 52 be needed to churn out enough ATP to power protein translation followed by an estimation of
 53 how many electron transport complexes must be present to maintain the proton motive force.
 54 A third class of estimates considers the need to maintain the size and shape of the cell through
 55 the construction of new lipids for the cell membranes as well as the glycan polymers which make
 56 up the rigid peptidoglycan. Our final class of hypotheses centers on the synthesis of a variety of
 57 biomolecules. Our focus is primarily on the stages of the central dogma as we estimate the number
 58 of protein complexes needed for DNA replication, transcription, and protein translation.

59 In broad terms, we find that the majority of these estimates are in close agreement with the
 60 experimental observations, with protein copy numbers apparently well-tuned for the task of cell
 61 doubling. This allows us to systematically scratch off the hypotheses diagrammed in **Figure 1** as
 62 setting possible speed limits. Ultimately, we find that protein translation (particularly the genera-
 63 tion of new ribosomes) acts as 1) a rate limiting step for the *fastest* bacterial division, and 2) the
 64 major determinant of bacterial growth across all nutrient conditions we have considered under
 65 steady state, exponential growth. This perspective is in line with the linear correlation observed
 66 between growth rate and ribosomal content (typically quantified through the ratio of RNA to pro-
 67 tein) for fast growing cells (*Scott et al., 2010*), but suggests a more prominent role for ribosomes
 68 in setting the doubling time across all conditions of nutrient limitation. Here we again leverage the
 69 quantitative nature of this data set and present a quantitative model of the relationship between
 70 the fraction of the proteome devoted to ribosomes and the speed limit of translation, revealing
 71 a fundamental tradeoff between the translation capacity of the ribosome pool and the maximal
 72 growth rate.

73 Uptake of Nutrients

74 In order to build new cellular mass, the molecular and elemental building blocks must be scav-
 75 enged from the environment in different forms. Carbon, for example, is acquired via the transport
 76 of carbohydrates and sugar alcohols with some carbon sources receiving preferential treatment
 77 in their consumption (*Monod, 1947*). Phosphorus, sulfur, and nitrogen, on the other hand, are har-
 78 vested primarily in the forms of inorganic salts, namely phosphate, sulfate, and ammonia (*Jun et al.,
 79 2018; Assentoft et al., 2016; Stasi et al., 2019; Antonenko et al., 1997; Rosenberg et al., 1977; Will-
 80 sky et al., 1973*). All of these compounds have different permeabilities across the cell membrane
 81 (*Phillips 2018*) and most require some energetic investment either via ATP hydrolysis or through
 82 the proton electrochemical gradient to bring the material across the hydrophobic cell membrane.
 83 Given the diversity of biological transport mechanisms and the vast number of inputs needed to
 84 build a cell, we begin by considering transport of some of the most important cellular ingredients:
 85 carbon, nitrogen, oxygen, hydrogen, phosphorus, and sulfur.

86 The elemental composition of *E. coli* has received much quantitative attention over the past
 87 half century (*Neidhardt et al., 1991; Taymaz-Nikerel et al., 2010; Heldal et al., 1985; Bauer and
 88 Ziv, 1976*), providing us with a starting point for estimating the copy numbers of various trans-
 89 porters. While there is some variability in the exact elemental percentages (with different uncer-
 90 tainties), we can estimate that the dry mass of a typical *E. coli* cell is \approx 45% carbon (BNID: 100649,
 91 *Milo et al. (2010)*), \approx 15% nitrogen (BNID: 106666, *Milo et al. (2010)*), \approx 3% phosphorus (BNID:

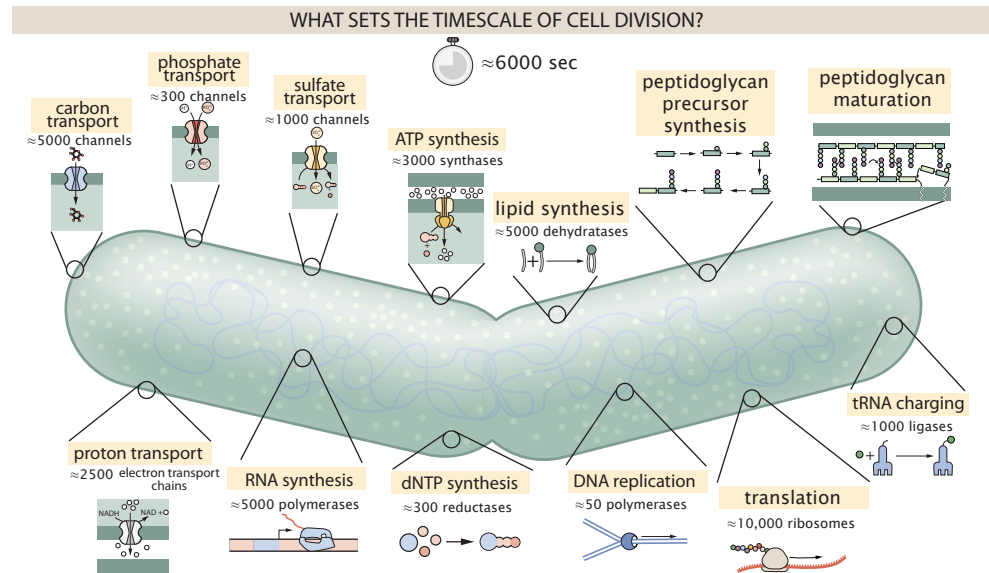


Figure 1. Transport and synthesis processes necessary for cell division. We consider an array of processes necessary for a cell to double its molecular components. Such processes include the transport of carbon across the cell membrane, the production of ATP, and fundamental processes of the central dogma namely RNA, DNA, and protein synthesis. A schematic of each synthetic or transport category is shown with an approximate measure of the complex abundance at a growth rate of 0.5 per hour. In this work, we consider a standard bacterial division time of ≈ 5000 sec.

92 100653, *Milo et al. (2010)*), and 1% sulfur (BNID: 100655, *Milo et al. (2010)*). In the coming para-
 93 graphs, we will engage in a dialogue between back-of-the-envelope estimates for the numbers of
 94 transporters needed to facilitate these chemical stoichiometries and the experimental proteomic
 95 measurements of the biological reality. Such an approach provides the opportunity to test if our
 96 biological knowledge is sufficient to understand the scale at which these complexes are produced.
 97 Specifically, we will make these estimates considering a modest doubling time of 5000 s, a growth
 98 rate of $\approx 0.5 \text{ hr}^{-1}$, the range in which the majority of the experimental measurements reside.

99 Nitrogen Transport

100 Before we begin our back-of-the-envelope estimations, we must address which elemental sources
 101 must require proteinaceous transport, meaning that the cell cannot acquire appreciable amounts
 102 simply via diffusion from the membrane. The permeability of the lipid membrane to a large num-
 103 ber of solutes has been extensively characterized over the past century. Large, polar molecular
 104 species (such as various sugar molecules, sulfate, and phosphate) have low permeabilities while
 105 small, non-polar compounds (such as oxygen, carbon dioxide, and ammonia) can readily diffuse
 106 across the membrane. Ammonia, a primary source of nitrogen in typical laboratory conditions,
 107 has a permeability on par with water ($\approx 10^5 \text{ nm/s}$, BNID:110824 *Milo et al. (2010)*). In particularly
 108 nitrogen-poor conditions, *E. coli* expresses a transporter (AmtB) which appears to aid in nitrogen
 109 assimilation, though the mechanism and kinetic details of transport is still a matter of debate (*van*
 110 *Heeswijk et al., 2013; Khademi et al., 2004*). Beyond ammonia, another plentiful source of nitrogen
 111 come in the form of glutamate, which has its own complex metabolism and scavenging pathways.
 112 However, nitrogen is plentiful in the growth conditions examined in this work, permitting us to ne-
 113 glect nitrogen transport as a potential rate limiting process in cell division in typical experimental
 114 conditions. We direct the reader to the supplemental information for a more in-depth discussion of
 115 permeabilities and a series of calculations revealing that active nitrogen transport can be neglected
 116 for the purposes of this article.

117 **Carbon Transport**

118 We begin our estimations with the most abundant element in *E. coli* by mass, carbon. Using ≈ 0.3
 119 pg as the typical *E. coli* dry mass (BNID: 103904, *Milo et al. (2010)*), we estimate that $\approx 10^{10}$ carbon
 120 atoms must be brought into the cell in order to double all of the carbon-containing molecules (*Fig-*
 121 *ure 2(A, top)*). Typical laboratory growth conditions, such as those explored in the aforementioned
 122 proteomic data sets, provide carbon as a single class of sugar such as glucose, galactose, or xylose
 123 to name a few. *E. coli* has evolved myriad mechanisms by which these sugars can be transported
 124 across the cell membrane. One such mechanism of transport is via the PTS system which is a
 125 highly modular system capable of transporting a diverse range of sugars (*Escalante et al., 2012*).
 126 The glucose-specific component of this system transports ≈ 200 glucose molecules per second per
 127 transporter (BNID: 114686, *Milo et al. (2010)*). Making the assumption that this is a typical sugar
 128 transport rate, coupled with the need to transport 10^{10} carbon atoms, we arrive at the conclusion
 129 that on the order of 1,000 transporters must be expressed in order to bring in enough carbon
 130 atoms to divide in 5000 s, diagrammed in the top panel of *Figure 2(A)*. This estimate, along with
 131 the observed average number of the PTS system carbohydrate transporters present in the pro-
 132 teomic data sets (*Schmidt et al., 2016; Peebo et al., 2015; Valgepea et al., 2013; Li et al., 2014*), is
 133 shown in *Figure 2(A)*. While we estimate 1500 transporters are needed with a 5000 s division time,
 134 we can abstract this calculation to consider any particular growth rate given knowledge of the cell
 135 density and volume as a function of growth rate and direct the reader to the SI for more informa-
 136 tion. As revealed in *Figure 2(A)*, experimental measurements exceed the estimate by several fold,
 137 illustrating that transport of carbon in to the cell is not rate limiting for cell division. Abstracting
 138 this point estimate at 5000 s to a continuum of growth rates (grey line in *Figure 2(A)*) reveals an
 139 excess of transporters at other growth rates, though in rapid growth regimes, the abundance is
 140 below our simple estimate.

141 The estimate presented in *Figure 2(A)* neglects any specifics of the regulation of carbon trans-
 142 port system and presents a data-averaged view of how many carbohydrate transporters are present
 143 on average. Using the diverse array of growth conditions explored in the proteomic data sets, we
 144 can explore how individual carbon transport systems depend on the population growth rate. In
 145 *Figure 2(B)*, we show the total number of carbohydrate transporters specific to different carbon
 146 sources. A striking observation, shown in the top-left plot of *Figure 2(B)*, is the constancy in the
 147 expression of the glucose-specific transport systems. Additionally, we note that the total number
 148 of glucose-specific transporters is tightly distributed $\approx 10^4$ per cell, the approximate number of
 149 transporters needed to sustain rapid growth of several divisions per hour. This illustrates that *E.*
 150 *coli* maintains a substantial number of complexes present for transporting glucose which is known
 151 to be the preferential carbon source (*Monod, 1947; Liu et al., 2005; Aidelberg et al., 2014*).

152 It is now understood that a large number of metabolic operons are regulated with dual-input
 153 logic gates that are only expressed when glucose concentrations are low (mediated by cyclic-AMP
 154 receptor protein CRP) and the concentration of other carbon sources are elevated (*Gama-Castro*
 155 *et al., 2016; Zhang et al., 2014b*). A famed example of such dual-input regulatory logic is in the regu-
 156 lation of the *lac* operon which is only natively activated in the absence of glucose and the presence
 157 of allolactose, an intermediate in lactose metabolism (*Jacob and Monod, 1961*), though we now
 158 know of many other such examples (*Ireland et al., 2020; Gama-Castro et al., 2016; Belliveau et al.,*
 159 *2018*). This illustrates that once glucose is depleted from the environment, cells have a means to
 160 dramatically increase the abundance of the specific transporter needed to digest the next sugar
 161 that is present. Several examples of induced expression of specific carbon-source transporters
 162 are shown in *Figure 2(B)*. Points colored in red (labeled by red text-boxes) correspond to growth
 163 conditions in which the specific carbon source (glycerol, xylose, or fructose) is present. These plots
 164 show that, in the absence of the particular carbon source, expression of the transporters is main-
 165 tained on the order of $\sim 10^2$ per cell. However, when the transport substrate is present, expression
 166 is induced and the transporters become highly-expressed. The grey lines in *Figure 2(B)* show the

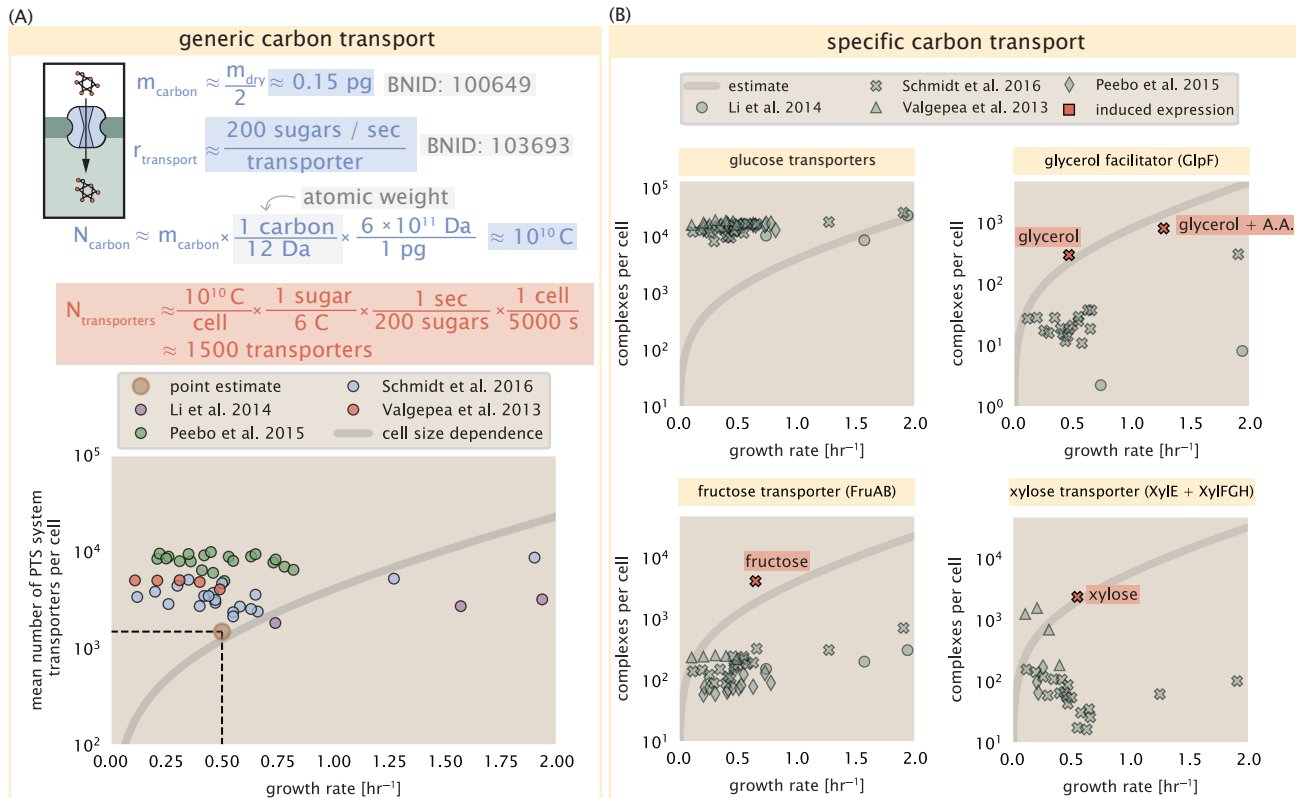


Figure 2. The abundance of carbon transport systems across growth rates. (A) A simple estimate for the minimum number of generic carbohydrate transport systems (top) assumes $\approx 10^{10}$ C are needed to complete division, each transported sugar contains ≈ 6 C, and each transporter conducts sugar molecules at a rate of ≈ 200 per second. Bottom plot shows the estimated number of transporters needed at a growth rate of ≈ 0.5 per hr (light-brown point and dashed lines). Colored points correspond to the mean number of PTS system sugar transporters (complexes annotated with the Gene Ontology term GO:0009401) for different growth conditions across different published datasets. (B) The abundance of various specific carbon transport systems plotted as a function of the population growth rate. The rates of substrate transport to compute the continuum growth rate estimate (grey line) were 200 glucose- s^{-1} (BNID: 103693, *Milo et al. (2010)*), 2000 glycerol- s^{-1} (*Lu et al., 2003*), 200 fructose- s^{-1} (assumed to be similar to PtsI, BNID: 103693, *Milo et al. (2010)*), and 50 xylose- s^{-1} (assumed to be comparable to LacY, BNID: 103159, *Milo et al. (2010)*). Red points and highlighted text indicate conditions in which the only source of carbon in the growth medium induces expression of the transport system. Grey line in (A) and (B) represents the estimated number of transporters per cell at a continuum of growth rates.

167 estimated number of transporters needed at each growth rate to satisfy the cellular carbon re-
 168 quirement. It is notable that in all cases, the magnitude of induced expression (shown in red) falls
 169 close to the estimate, illustrating the ability of the cell to tune expression in response to changing
 170 environments. Together, this generic estimation and the specific examples of induced expression
 171 suggest that transport of carbon across the cell membrane, while critical for growth, is not the
 172 rate-limiting step of cell division.

173 **Phosphorus and Sulfur Transport**

174 We now turn our attention towards other essential elements, namely phosphorus and sulfur. Phos-
 175 phorus is critical to the cellular energy economy in the form of high-energy phosphodiester bonds
 176 making up DNA, RNA, and the NTP energy pool as well as playing a critical role in the post-translational
 177 modification of proteins and defining the polar-heads of lipids. In total, phosphorus makes up
 178 $\approx 3\%$ of the cellular dry mass which in typical experimental conditions is in the form of inorganic
 179 phosphate. The cell membrane has remarkably low permeability to this highly-charged and critical
 180 molecule, therefore requiring the expression of active transport systems. In *E. coli*, the proton elec-
 181 trochemical gradient across the inner membrane is leveraged to transport inorganic phosphate
 182 into the cell (Rosenberg *et al.*, 1977). Proton-solute symporters are widespread in *E. coli* (Ramos
 183 and Kaback, 1977; Booth *et al.*, 1979) and can have rapid transport rates of 50 to 100 molecules
 184 per second for sugars and other solutes (BNID: 103159; 111777, Milo *et al.* (2010)). As a more
 185 extreme example, the proton transporters in the F₁-F₀ ATP synthase, which leverage the proton
 186 electrochemical gradient for rotational motion, can shuttle protons across the membrane at a rate
 187 of ≈ 1000 per second (BNID: 104890; 103390, (Milo *et al.*, 2010)). In *E. coli* the PitA phosphate trans-
 188 port system has been shown to be very tightly coupled with the proton electrochemical gradient
 189 with a 1:1 proton:phosphate stoichiometric ratio (Harris *et al.*, 2001; Feist *et al.*, 2007). Taking the
 190 geometric mean of the aforementioned estimates gives a plausible rate of phosphate transport
 191 on the order of 300 per second. Illustrated in *Figure 3(A)*, we can estimate that ≈ 150 phosphate
 192 transporters are necessary to maintain an $\approx 3\%$ dry mass with a 5000 s division time. This estimate
 193 is again satisfied when we examine the observed copy numbers of PitA in proteomic data sets (plot
 194 in *Figure 3(A)*). While our estimate is very much in line with the observed numbers, we emphasize
 195 that this is likely a slight overestimate of the number of transporters needed as there are other
 196 phosphorous scavenging systems, such as the ATP-dependent phosphate transporter Pst system
 197 which we have neglected.

198 Satisfied that there are a sufficient number of phosphate transporters present in the cell, we
 199 now turn to sulfur transport as another potentially rate limiting process. Similar to phosphate,
 200 sulfate is highly-charged and not particularly membrane permeable, requiring active transport.
 201 While there exists a H+/sulfate symporter in *E. coli*, it is in relatively low abundance and is not well
 202 characterized (Zhang *et al.*, 2014a). Sulfate is predominantly acquired via the ATP-dependent ABC
 203 transporter CysUWA system which also plays an important role in selenium transport (Sekowska
 204 *et al.*, 2000; Sirko *et al.*, 1995). While specific kinetic details of this transport system are not readily
 205 available, generic ATP transport systems in prokaryotes transport on the order of 1 to 10 molecules
 206 per second (BNID: 109035, Milo *et al.* (2010)). Combining this generic transport rate, measurement
 207 of sulfur comprising 1% of dry mass, and a 5000 second division time yields an estimate of ≈ 1000
 208 CysUWA complexes per cell (*Figure 3(B)*). Once again, this estimate is in notable agreement with
 209 proteomic data sets, suggesting that there are sufficient transporters present to acquire the nec-
 210 essary sulfur. In a similar spirit of our estimate of phosphorus transport, we emphasize that this is
 211 likely an overestimate of the number of necessary transporters as we have neglected other sulfur
 212 scavenging systems that are in lower abundance.

213 **Limits on Transporter Expression**

214 So which, if any, of these processes may be rate limiting for growth? As suggested by *Figure 2*
 215 (B), induced expression can lead to an order-of-magnitude (or more) increase in the amount of

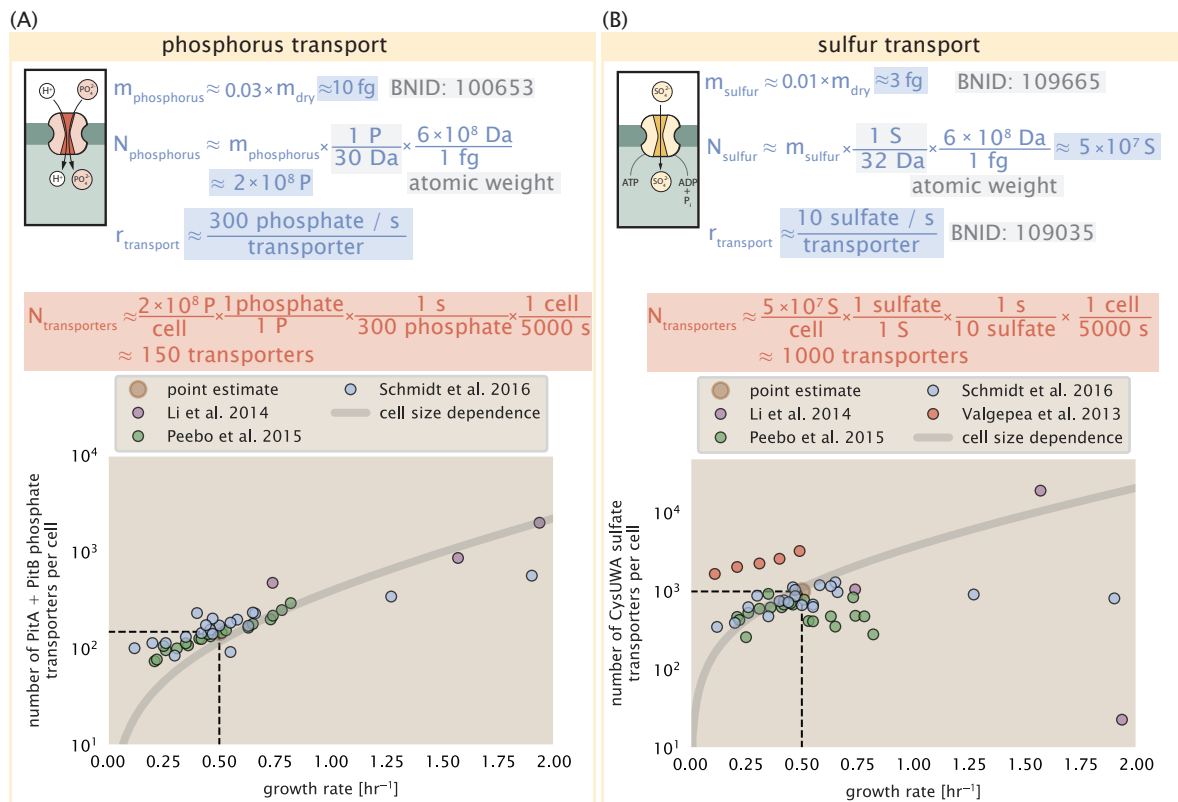


Figure 3. Estimates and measurements of phosphate and sulfate transport systems as a function of growth rate. (A) Estimate for the number of PitA phosphate transport systems needed to maintain a 3% phosphorus *E. coli* dry mass. Points in plot correspond to the total number of PitA transporters per cell. (B) Estimate of the number of CysUWA complexes necessary to maintain a 1% sulfur *E. coli* dry mass. Points in plot correspond to average number of CysUWA transporter complexes that can be formed given the transporter stoichiometry [CysA]₂[CysU][CysW][Sbp/CysP]. Grey line in (A) and (B) represents the estimated number of transporters per cell at a continuum of growth rates.

216 transporters needed to facilitate transport. Thus, if acquisition of nutrients was the limiting state
 217 in cell division, could expression simply be increased to accommodate faster growth? A way to
 218 approach this question is to compute the amount of space in the bacterial membrane that could
 219 be occupied by nutrient transporters. Considering a rule-of-thumb for the surface area of *E. coli* of
 220 about $6 \mu\text{m}^2$ (BNID: 101792, *Milo et al. (2010)*), we expect an areal density for 1000 transporters to
 221 be approximately 200 transporters/ μm^2 . For a typical transporter occupying about $50 \text{ nm}^2/\text{dimer}$,
 222 this amounts to about only 1 percent of the total inner membrane (*Szenk et al., 2017*). In addition,
 223 bacterial cell membranes typically have densities of 10^5 proteins/ μm^2 (*Phillips, 2018*), implying that
 224 the cell could accommodate more transporters of a variety of species if it were rate limiting. As we
 225 will see in the next section, however, occupancy of the membrane can impose other limits on the
 226 rate of energy production.

227 Energy Production

228 While the transport of nutrients is required to build new cell mass, the metabolic pathways both
 229 consume and generate energy in the form of NTPs. The high-energy phosphodiester bonds of
 230 (primarily) ATP power a variety of cellular processes that drive biological systems away from ther-
 231 modynamic equilibrium. The next set of processes we hypothesize might control the rate of cell
 232 division considers the energy budget of a dividing cell in terms of the synthesis of ATP from ADP
 233 and inorganic phosphate as well as maintenance of the electrochemical proton gradient which
 234 powers it.

235 ATP Synthesis

236 Hydrolysis of the terminal phosphodiester bond of ATP forming ADP and an inorganic phosphate is
 237 a kinetic driving force in a wide array of biochemical reactions. One such reaction is the formation
 238 of peptide bonds during translation which requires ≈ 2 ATPs for the charging of an amino acid
 239 to the tRNA and ≈ 2 ATP equivalents for the formation of the peptide bond between amino acids.
 240 Considering the ATP costs associated with error correction and post-translational modifications
 241 of proteins, we can make the approximation that each peptide bond has a net cost of ≈ 5 ATP
 242 (BNID: 107782, *Milo et al. (2010)*). In total, the energetic costs of peptide bond formation consume
 243 $\approx 80\%$ of the cells ATP budget (BNID: 107782; 106158; 101637; 111918, *Milo et al. (2010); Lynch*
and Marinov (2015); Stouthamer (1973)). The pool of ATP is produced by the F₁-F₀ ATP synthase
 245 – a membrane-bound rotary motor which under ideal conditions can yield ≈ 300 ATP per second
 246 (BNID: 114701; *Milo et al. (2010); Weber and Senior (2003)*).

247 To estimate the total number of ATP equivalents consumed during a cell cycle, we will make
 248 the approximation that there are $\approx 3 \times 10^6$ proteins per cell with an average protein length of ≈ 300
 249 peptide bonds (BNID: 115702; 108986; 104877, *Milo et al. (2010)*). Taking these values together,
 250 we estimate that the typical *E. coli* cell consumes $\approx 5 \times 10^9$ ATP per cell cycle on protein synthesis
 251 alone and $\approx 6 \times 10^9$ ATP in total. Assuming that the ATP synthases are operating at their fastest
 252 possible rate, ≈ 3000 ATP synthases are needed to keep up with the energy demands of the cell.
 253 This estimate and a comparison with the data are shown in *Figure 4* (A). Despite our assumption
 254 of maximal ATP production rate per synthase and approximation of all NTP consuming reactions
 255 being the same as ATP, we find that an estimate of a few thousand complete synthases per cell
 256 to agree well with the experimental data. Much as we did for the estimates of transporter copy
 257 number in the previous section, we can generalize this estimation to consider a continuum of
 258 growth rates rather than a point estimate of 5000 s, indicated by the gray lines in *Figure 4*, and find
 259 that this approach adequately describes the observed growth rate dependence.

260 If the direct production of ATP was a rate limiting step for growth, could the cell simply express
 261 more ATP synthase complexes? This requires us to consider several features of cellular physiology,
 262 namely the physical space on the inner membrane as well as the ability to maintain the proton
 263 chemical gradient leveraged by the synthase to drive ATP production out of equilibrium.

264 Generating the Proton Electrochemical Gradient

265 In order to produce ATP, the F₁-F₀ ATP synthase itself must consume energy. Rather than burning
 266 through its own product, this intricate macromolecular machine has evolved to exploit the elec-
 267 trochemical potential established across the inner membrane through cellular respiration. This
 268 electrochemical gradient is manifest by the pumping of protons into the intermembrane space via
 269 the electron transport chains as they reduce NADH. In *E. coli*, this potential difference is ≈ -200 mV
 270 (BNID: 102120, *Milo et al. (2010)*). A simple estimate of the inner membrane as a capacitor with a
 271 working voltage of -200 mV (as performed in the Supplemental Information) reveals that $\approx 2 \times 10^4$
 272 protons must be present in the intermembrane space.

273 However, the constant rotation of the ATP synthases would rapidly abolish this potential dif-
 274 ference if it were not being actively maintained. To undergo a complete rotation (and produce a
 275 single ATP), the F₁-F₀ ATP synthase must shuttle ≈ 4 protons across the membrane into the cytosol
 276 (BNID: 103390, *Milo et al. (2010)*). With ≈ 3000 ATP synthases each generating 300 ATP per second,
 277 the 2×10^4 protons establishing the 200 mV potential would be consumed in only a few millisec-
 278 onds. This brings us to our next estimate: how many electron transport complexes are needed to
 279 support the consumption rate of the ATP synthases?

280 The electrochemistry of the electron transport complexes of *E. coli* have been the subject of
 281 intense biochemical and biophysical study over the past half century (*Ingledew and Poole, 1984;*
282 Khademian and Imlay, 2017; Cox et al., 1970; Henkel et al., 2014). A recent work (*Szenk et al.,*
283 2017) examined the respiratory capacity of the *E. coli* electron transport complexes using struc-
 284 tural and biochemical data, revealing that each electron transport chain rapidly pumps protons
 285 into the intermembrane space at a clip of ≈ 1500 protons per second (BIND: 114704; 114687, *Milo*
286 et al. (2010)). Using our estimate of the number of ATP synthases required per cell (*Figure 4(A)*),
 287 coupled with these recent measurements, we estimate that ≈ 1000 electron transport complexes
 288 would be necessary to facilitate the $\approx 4 \times 10^6$ protons per second diet of the cellular ATP synthases.
 289 This estimate (along with a generalization to the entire range of observed growth rates) is in agree-
 290 ment with the number of complexes identified in the proteomic datasets (plot in *Figure 4(B)*). This
 291 suggests that every ATP synthase must be accompanied by ≈ 1 functional electron transport chain.
 292 Again, if this were a rate limiting process for bacterial growth, one must conclude that it is not
 293 possible for the cell to simply increase the production of both the number of electron transport
 294 chain complexes as well as ATP synthases. As both of these components only function bound to
 295 the inner membrane, we now turn our attention towards the available space in the membrane as
 296 well as surface-area-to-volume constraints.

297 Energy Production in a Crowded Membrane.

298 For each protein considered so far, the data shows that in general their numbers increase with
 299 growth rate. This is in part a consequence of the increase in cell length and width at that is common
 300 to many rod-shaped bacteria at faster growth rates (*Ojikic et al., 2019; Harris and Theriot, 2018*).
 301 For the particular case of *E. coli*, the total cellular protein and cell size increase logarithmically
 302 with growth rate (*Schaechter et al., 1958; Si et al., 2017*). Indeed, this is one reason why we have
 303 considered only a single, common growth condition across all our estimates so far. Such a scaling
 304 will require that the total number of proteins and net demand on resources also grow in proportion
 305 to the increase in cell size divided by the cell's doubling time. Recall however that each transport
 306 process, as well as the ATP production via respiration, is performed at the bacterial membrane.
 307 This means that their maximum productivity can only increase in proportion to the cell's surface
 308 area divided by the cell doubling time. This difference in scaling would vary in proportion to the
 309 surface area-to-volume (S/V) ratio.

310 While we found that there was more than sufficient membrane real estate for carbon intake in
 311 our earlier estimate, the total number of ATP synthases and electron chain transport complexes
 312 both exhibit a clear increase in copy number with growth rate, reaching in excess of 10^4 copies per
 313 cell (*Figure 4*). Here we consider the consequences of this S/V ratio scaling in more detail.

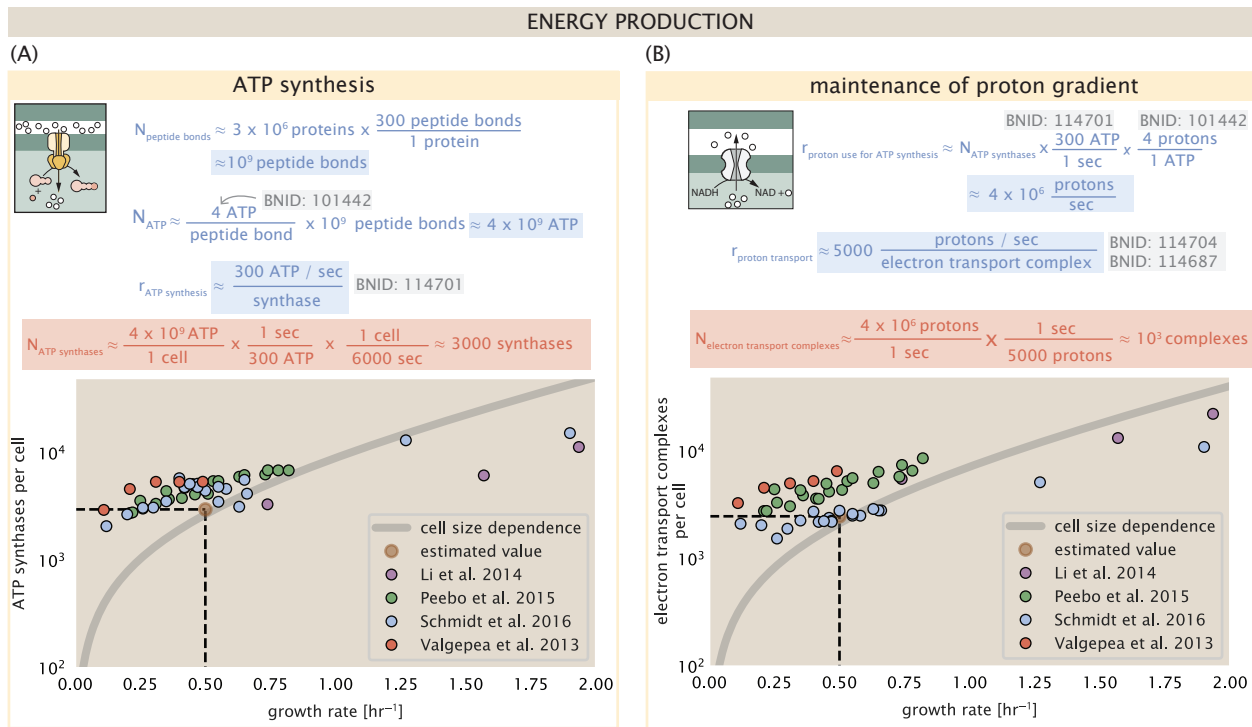


Figure 4. The abundance of F₁-F₀ ATP synthases and electron transport chain complexes as a function of growth rate. (A) Estimate of the number of F₁-F₀ ATP synthase complexes needed to accommodate peptide bond formation and other NTP dependent processes. Points in plot correspond to the mean number of complete F₁-F₀ ATP synthase complexes that can be formed given proteomic measurements and the subunit stoichiometry [AtpE]₁₀[AtpF]₂[AtpB][AtpC][AtpH][AtpA]₃[AtpG][AtpD]₃. (B) Estimate of the number of electron transport chain complexes needed to maintain a membrane potential of -200 mV given estimate of number of F₁-F₀ ATP synthases from (A). Points in plot correspond to the average number of complexes identified as being involved in aerobic respiration by the Gene Ontology identifier GO:0019646 that could be formed given proteomic observations. These complexes include cytochromes *bd1* ([CydA][CydB][CydX][CydH]), *bdII* ([AppC][AppB]), *bo3*, ([CyoD][CyoA][CyoB][CyoC]) and NADH:quinone oxioreductase I ([NuoA][NuoH][NuoJ][NuoK][NuoL][NuoM][NuoN][NuoB][NuoC][NuoE][NuoF][NuoG][NuoI]) and II ([Ndh]). Grey lines in both (A) and (B) correspond to the estimate procedure described, but applied to a continuum of growth rates. We direct the reader to the Supporting Information for a more thorough description of this approach.

314 In our estimate of ATP production above we found that a cell demands about 6×10^9 ATP or 10^6
 315 ATP/s. With a cell volume of roughly 1 fL, this corresponds to about 2×10^{10} ATP per fL of cell volume,
 316 in line with previous estimates (*Stouthamer and Bettenhausen, 1977; Szenk et al., 2017*). In **Figure 5**(A) we plot this ATP demand as a function of the S/V ratio in green, where we have considered
 317 a range of cell shapes from spherical to rod-shaped with an aspect ratio (length/width) equal to 4
 318 (See appendix for calculations of cell volume and surface area). In order to consider the maximum
 319 power that could be produced, we consider the amount of ATP that can be generated by a membrane
 320 filled with ATP synthase and electron transport complexes, which provides a maximal production
 321 of about 3 ATP / (nm²·s) (*Szenk et al., 2017*). This is shown in blue in **Figure 5**(A), which shows that
 322 at least for the growth rates observed, the energy demand is roughly an order of magnitude less.
 323

324 Interestingly, *Szenk et al.* (2017) also found that ATP production by respiration is less efficient
 325 than by fermentation per membrane area occupied due to the additional proteins of the electron
 326 transport chain. This suggests that even under anaerobic growth, there will be sufficient mem-
 327 brane space for ATP production in general.

328 While this serves to highlight the diminishing capacity to provide resources to grow if the cell
 329 increases in size (and its S/V decreases), the blue region in **Figure 5**(A) represents a somewhat
 330 unachievable limit since the inner membrane must also include other proteins such as those re-
 331 quired for lipid and membrane synthesis. To gain insight, we used the proteomic data to look at
 332 the distribution of proteins on the inner membrane. Here we use Gene Ontology (GO) annotations
 333 (*Ashburner et al., 2000; The Gene Ontology Consortium, 2018*) to identify all proteins embedded
 334 or peripheral to the inner membrane (GO term: 0005886). Those associated but not membrane-
 335 bound include proteins like MreB and FtsZ, that traverse the inner membrane by treadmilling and
 336 must nonetheless be considered as a vital component occupying space on the membrane. In **Fig-**
 337 **ure 5**(B), we find that the total protein mass per μm^2 is relatively constant with growth rate. Inter-
 338 estingly, when we consider the distribution of proteins grouped by their Clusters of Orthologous
 339 Groups (COG) (*Tatusov et al., 2000*), the relative abundance for those in metabolism (including ATP
 340 synthesis via respiration) is also relatively constant.

341 Function of the Central Dogma

342 Up to this point, we have considered a variety of transport and biosynthetic processes that are
 343 critical to acquiring and generating new cell mass. While there are of course many other metabolic
 344 processes we could consider and perform estimates of (such as the components of fermentative
 345 versus aerobic respiration), we now turn our focus to some of the most central processes which
 346 *must* be undertaken irrespective of the growth conditions – the processes of the central dogma.

347 DNA

348 Most bacteria (including *E. coli*) harbor a single, circular chromosome and can have extra-chromosomal
 349 plasmids up to ~ 100 kbp in length. We will focus our quantitative thinking solely on the chromo-
 350 some of *E. coli* which harbors ≈ 5000 genes and $\approx 5 \times 10^6$ base pairs. To successfully divide and
 351 produce viable progeny, this chromosome must be faithfully replicated and segregated into each
 352 nascent cell. We again rely on the near century of literature in molecular biology to provide some
 353 insight on the rates and mechanics of the replicative feat as well as the production of the required
 354 starting materials, dNTPs.

355 dNTP synthesis

356 We begin our exploration of DNA replication by examining the production of the deoxyribonucleotide
 357 triphosphates (dNTPs). The four major dNTPs (dATP, dTTP, dCTP, and dGTP) are synthesized *de*
 358 *novo* in separate pathways, requiring different building blocks. However, a critical step present in
 359 all dNTP synthesis pathways is the conversion from ribonucleotide to deoxyribonucleotide via the
 360 removal of the 3' hydroxyl group of the ribose ring (*Rudd et al., 2016*). This reaction is mediated
 361 by a class of enzymes termed ribonucleotide reductases, of which *E. coli* possesses two aerobically

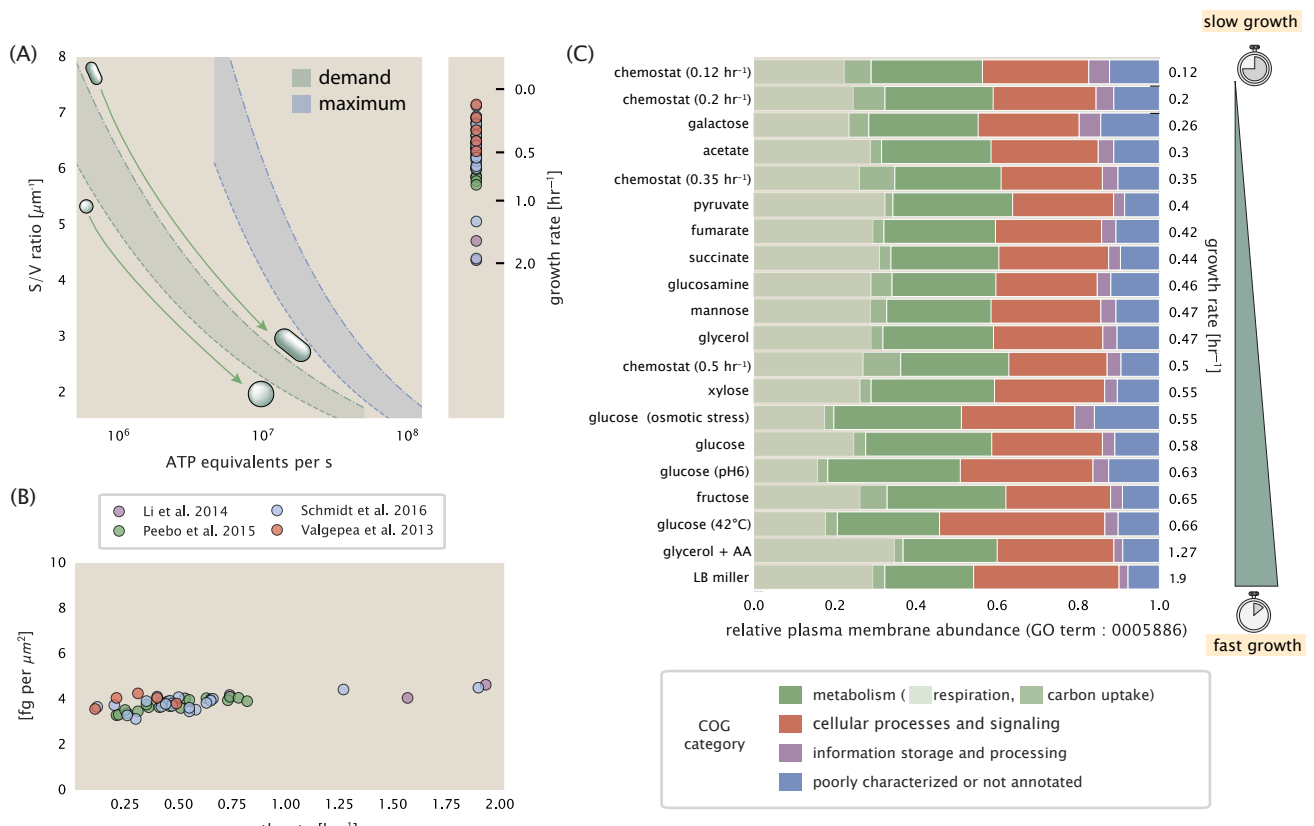


Figure 5. Influence of cell size and S/V ratio on ATP production and inner membrane composition. (A) Scaling of ATP demand and maximum ATP production as a function of S/V ratio. Cell volumes of 0.5 fL to 50 fL were considered, with the dashed (—) line corresponding to a sphere and the dash-dot line (---) reflecting a rod-shaped bacterium like *E. coli* with a typical aspect ratio (length / width) of 0.4 (Shi et al., 2018). Approximately 50% of the bacterial inner membrane is assumed to be protein, with the remainder lipid. (B) Total protein mass calculated for proteins with inner membrane annotation (GO term: 0005886). (C) Relative protein abundances by mass based on COG annotation. Metabolic proteins are further separated into respiration (F_1 - F_0 ATP synthase, NADH dehydrogenase I, succinate:quinone oxidoreductase, cytochrome bo₃ ubiquinol oxidase, cytochrome bd-I ubiquinol oxidase) and carbohydrate transport (GO term: GO:0008643). Note that the elongation factor EF-Tu can also associate with the inner membrane, but was excluded in this analysis due to its high relative abundance (roughly identical to the total mass shown in part (B)).

362 active complexes (termed I and II) and a single anaerobically active enzyme. Due to their peculiar
 363 formation of a radical intermediate, these enzymes have received much biochemical, kinetic, and
 364 structural characterization. One such work (**Ge et al., 2003**) performed a detailed *in vitro* measure-
 365 ment of the steady-state kinetic rates of these complexes, revealing a turnover rate of ≈ 10 dNTP
 366 per second.

367 Since this reaction is central to the synthesis of all dNTPs, it is reasonable to consider the abun-
 368 dence of these complexes is a measure of the total dNTP production in *E. coli*. Illustrated schemati-
 369 cally in **Figure 6** (A), we consider the fact that to replicate the cell's genome, on the order of $\approx 10^7$
 370 dNTPs must be synthesized. Assuming a production rate of 10 per second per ribonucleotide
 371 reductase complex and a cell division time of 5000 seconds, we arrive at an estimate of ≈ 200
 372 complexes needed per cell. As shown in the bottom panel of **Figure 6** (A), this estimate agrees
 373 with the experimental measurements of these complexes abundances within $\approx 1/2$ an order of
 374 magnitude. Extension of this estimate across a continuum of growth rate, including the fact that
 375 multiple chromosomes can be replicated at a given time, is shown as a grey transparent line in
 376 **Figure 6** (A). Similarly to our point estimate, this refinement agrees well with the data, accurately
 377 describing both the magnitude of the complex abundance and the dependence on growth rate.

378 Recent work has revealed that during replication, the ribonucleotide reductase complexes co-
 379 alesce to form discrete foci colocalized with the DNA replisome complex (**Sánchez-Romero et al.,**
 380 **2011**). This is particularly pronounced in conditions where growth is slow, indicating that spatial
 381 organization and regulation of the activity of the complexes plays an important role.

382 DNA Replication

383 We now turn our focus to the integration of these dNTP building blocks into the replicated chromo-
 384 some strand via the DNA polymerase. Replication is initiated at a single region of the chromosome
 385 termed the *oriC* locus at which a pair of DNA polymerases bind and begin their high-fidelity repli-
 386 cation of the genome in opposite directions. Assuming equivalence between the two replication
 387 forks, this means that the two DNA polymerase complexes (termed replisomes) meet at the mid-
 388 way point of the circular chromosome termed the *ter* locus. The kinetics of the five types of DNA
 389 polymerases (I – V) have been intensely studied, revealing that DNA polymerase III performs the
 390 high fidelity processive replication of the genome with the other "accessory" polymerases playing
 391 auxiliary roles (**Fijalkowska et al., 2012**). *In vitro* measurements have shown that DNA Polymerase
 392 III copies DNA at a rate of ≈ 600 nucleotides per second (BNID: 104120, **Milo et al. (2010)**). There-
 393 fore, to replicate a single chromosome, two replisomes (containing two DNA polymerase III each)
 394 moving at their maximal rate would copy the entire genome in ≈ 4000 s. Thus, with a division time
 395 of 5000 s (our "typical" growth rate for the purposes of this work), there is sufficient time for a pair
 396 of replisomes complexes to replicate the entire genome. However, this estimate implies that 4000
 397 s would be the upper-limit time scale for bacterial division which is at odds with the familiar 20
 398 minute (1200 s) doubling time of *E. coli* in rich medium.

399 It is well known that *E. coli* can parallelize its DNA replication such that multiple chromosomes
 400 are being replicated at once, with as many as 10 - 12 replication forks at a given time (**Bremer**
 401 **and Dennis, 2008; Si et al., 2017**). Thus, even in rapidly growing cultures, we expect only a few
 402 polymerases (≈ 10) are needed to replicate the chromosome per cell doubling. However, as shown
 403 in **Figure 6** (B), DNA polymerase III is nearly an order of magnitude more abundant. This
 404 discrepancy can be understood by considering its binding constant to DNA. DNA polymerase III is
 405 highly processive, facilitated by a strong affinity of the complex to the DNA. *In vitro* biochemical
 406 characterization has quantified the K_D of DNA polymerase III holoenzyme to single-stranded and
 407 double-stranded DNA to be 50 and 200 nM, respectively (**Ason et al., 2000**). The bottom plot in
 408 **Figure 6** (B) shows that the concentration of the DNA polymerase III across all data sets and growth
 409 conditions is within this range. Thus, while the copy number of the DNA polymerase III is in excess
 410 of the strict number required to replicate the genome, its copy number appears to vary such that its
 411 concentration is approximately equal to the dissociation constant to the DNA. While the processes

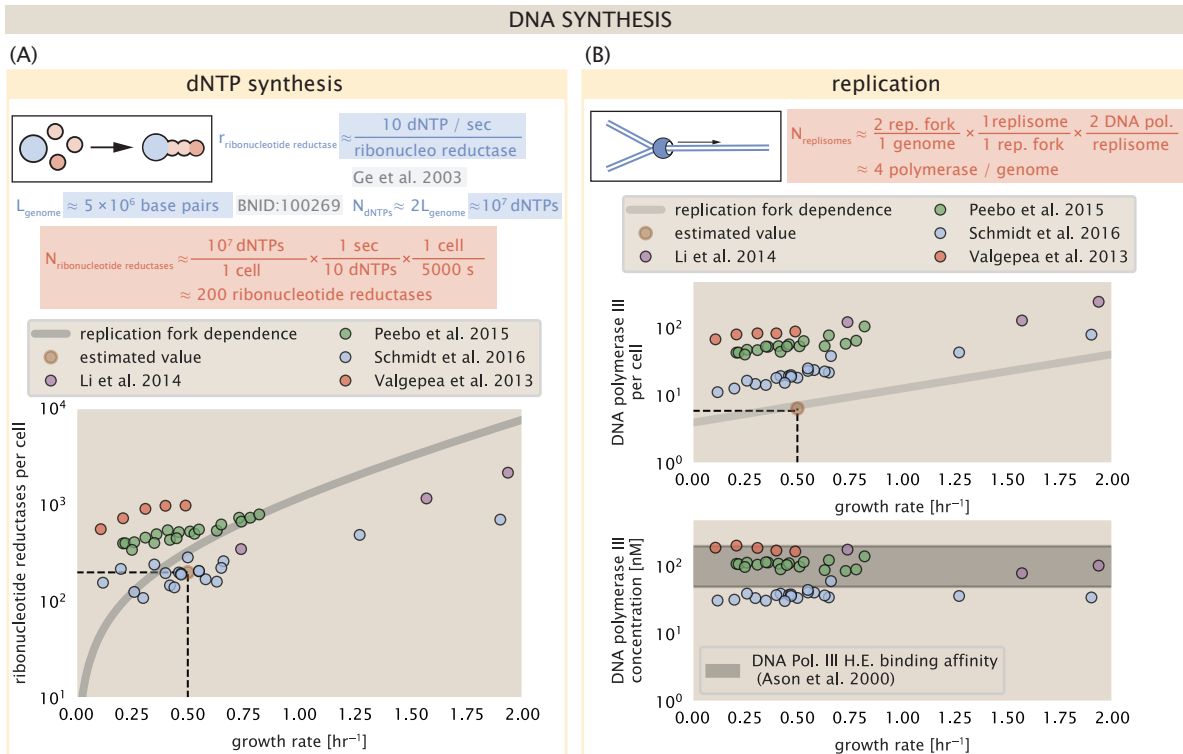


Figure 6. Complex abundance estimates for dNTP synthesis and DNA replication. (A) Estimate of the number of ribonucleotide reductase enzymes needed to facilitate the synthesis of $\approx 10^7$ dNTPs over the course of a 5000 second generation time. Points in the plot correspond to the total number of ribonucleotide reductase I ($[\text{NrdA}]_2[\text{NrdB}]_2$) and ribonucleotide reductase II ($[\text{NrdE}]_2[\text{NrdF}]_2$) complexes. (B) An estimate for the minimum number of DNA polymerase holoenzyme complexes needed to facilitate replication of a single genome. Points in the top plot correspond to the total number of DNA polymerase III holoenzyme complexes ($[\text{DnaE}]_3[\text{DnaQ}]_3[\text{HolE}]_3[\text{DnaX}]_5[\text{HolB}][\text{HolA}][\text{DnaN}]_4[\text{HolC}]_4[\text{HolD}]_4$) per cell. Bottom plot shows the effective concentration of DNA polymerase III holoenzyme given cell volumes calculated from the growth rate as in *Si et al. (2019)* (See Supplemental Information Section 4). Grey lines in (A) and top panel of (B) show the estimated number of complexes needed as a function of growth, the details of which are described in the Supplemental Information.

regulating the initiation of DNA replication are complex and involve more than just the holoenzyme, these data indicate that the kinetics of replication rather than the explicit copy number of the DNA polymerase III holoenzyme is the more relevant feature of DNA replication to consider. In light of this, the data in **Figure 6(B)** suggests that for bacteria like *E. coli*, DNA replication does not represent a rate-limiting step in cell division. However, it is worth noting that for bacterium like *C. crescentus* whose chromosomal replication is initiated only once per cell cycle (*Jensen et al., 2001*), the time to double their chromosome likely represents an upper limit to their growth rate.

RNA Synthesis

With the machinery governing the replication of the genome accounted for, we now turn our attention to the next stage of the central dogma – the transcription of DNA to form RNA. We primarily consider three major groupings of RNA, namely the RNA associated with ribosomes (rRNA), the RNA encoding the amino-acid sequence of proteins (mRNA), and the RNA which links codon sequence to amino-acid identity during translation (tRNA). Despite the varied function of these RNA species, they share a commonality in that they are transcribed from DNA via the action of RNA polymerase. In the coming paragraphs, we will consider the synthesis of RNA as a rate limiting step in bacterial division by estimating how many RNA polymerases must be present to synthesize all necessary rRNA, mRNA, and tRNA.

rRNA

We begin with an estimation of the number of RNA polymerases needed to synthesize the rRNA that serve as catalytic and structural elements of the ribosome. Each ribosome contains three rRNA molecules of lengths 120, 1542, and 2904 nucleotides (BNID: 108093, *Milo et al. (2010)*), meaning each ribosome contains ≈ 4500 nucleotides. As the *E. coli* RNA polymerase transcribes DNA to RNA at a rate of ≈ 40 nucleotides per second (BNID: 101904, *Milo et al. (2010)*), it takes a single RNA polymerase ≈ 100 s to synthesize the RNA needed to form a single functional ribosome. Therefore, in a 5000 s division time, a single RNA polymerase transcribing rRNA at a time would result in only ≈ 50 functional ribosomal rRNA units – far below the observed number of $\approx 10^4$ ribosomes per cell.

Of course, there can be more than one RNA polymerase transcribing the rRNA genes at any given time. To elucidate the *maximum* number of rRNA units that can be synthesized given a single copy of each rRNA gene, we will consider a hypothesis in which the rRNA operon is completely tiled with RNA polymerase. *In vivo* measurements of the kinetics of rRNA transcription have revealed that RNA polymerases are loaded onto the promoter of an rRNA gene at a rate of ≈ 1 per second (BNID: 111997; 102362, *Milo et al. (2010)*). If RNA polymerases are being constantly loaded on to the rRNA genes at this rate, then we can assume that ≈ 1 functional rRNA unit is synthesized per second. With a 5000 second division time, this hypothesis leads to a maximal value of 5000 functional rRNA units, still undershooting the observed number of 10^4 ribosomes per cell.

E. coli has evolved a clever mechanism to surpass this kinetic limit for the rate of rRNA production. Rather than having only one copy of each rRNA gene, *E. coli* has seven copies of the operon (BIND: 100352, *Milo et al. (2010)*) four of which are localized directly adjacent to the origin of replication (*Birnbaum and Kaplan, 1971*). As fast growth also implies an increased gene dosage due to parallelized chromosomal replication, the total number of rRNA genes can be on the order of $\approx 10 - 70$ copies at moderate to fast growth rates (*Stevenson and Schmidt, 2004*). Using our standard time scale of a 5000 second division time, we can make the lower-bound estimate that the typical cell will have 7 copies of the rRNA operon. Synthesizing one functional rRNA unit per second per rRNA operon, a total of 4×10^4 rRNA units can be synthesized, comfortably above the observed number of ribosomes per cell.

How many RNA polymerases are then needed to constantly transcribe 7 copies of the rRNA genes? We approach this estimate by considering the maximum number of RNA polymerases tiled along the rRNA genes with a loading rate of 1 per second and a transcription rate of 40 nucleotides per second. Considering that a RNA polymerase has a physical footprint of approximately 40 nu-

461 cleotides (BNID: 107873, *Milo et al. (2010)*), we can expect ≈ 1 RNA polymerase per 80 nucleotides.
462 With a total length of ≈ 4500 nucleotides per operon and 7 operons per cell, the maximum number
463 of RNA polymerases that can be transcribing rRNA at any given time is ≈ 400 . As we will see in the
464 coming sections, the synthesis of rRNA is the dominant requirement of the RNA polymerase pool.

465 mRNA

466 To form a functional protein, all protein coding genes must first be transcribed from DNA to form
467 an mRNA molecule. While each protein requires an mRNA blueprint, many copies of the protein
468 can be synthesized from a single mRNA. Factors such as strength of the ribosomal binding site,
469 mRNA stability, and rare codon usage frequency dictate the number of proteins that can be made
470 from a single mRNA, with yields ranging from 10^1 to 10^4 (BNID: 104186; 100196; 106254, *Milo et al.*
471 (2010)). Computing the geometric mean of this range yields ≈ 1000 proteins synthesized per mRNA,
472 a value that agrees with experimental measurements of the number of proteins per cell ($\approx 3 \times 10^6$,
473 BNID: 100088, *Milo et al. (2010)*) and total number of mRNA per cell ($\approx 3 \times 10^3$, BNID:100064, *Milo*
474 *et al. (2010)*).

475 This estimation captures the *steady-state* mRNA copy number, meaning that at any given time,
476 there will exist approximately 3000 unique mRNA molecules. To determine the *total* number of
477 mRNA that need to be synthesized over the cell's lifetime, we must consider degradation of the
478 mRNA. In most bacteria, mRNAs are rather unstable with life times on the order of several minutes
479 (BNID: 104324; 106253; 111927; 111998, *Milo et al. (2010)*). For convenience, we assume that the
480 typical mRNA in our cell of interest has a typical lifetime of ≈ 300 seconds. Using this value, we
481 can determine the total mRNA production rate to maintain a steady-state copy number of 3000
482 mRNA per cell. While we direct the reader to the appendix for a more detailed discussion of mRNA
483 transcriptional dynamics, we state here that the total mRNA production rate must be on the order
484 of ≈ 15 mRNA per second. In *E. coli*, the average protein is ≈ 300 amino acids in length (BNID:
485 108986; *Milo et al. (2010)*), meaning that the corresponding mRNA is ≈ 900 nucleotides which we
486 will further approximate as ≈ 1000 nucleotides to account for the non-protein coding regions on
487 the 5' and 3' ends. This means that the cell must have enough RNA polymerase molecules about
488 to sustain a transcription rate of $\approx 1.5 \times 10^4$ nucleotides per second. Knowing that a single RNA
489 polymerase polymerizes RNA at a clip of 40 nucleotides per second, we arrive at a comfortable
490 estimate of ≈ 250 RNA polymerase complexes needed to satisfy the mRNA demands of the cell. It
491 is worth noting that this number is approximately half of that required to synthesize enough rRNA,
492 as we saw in the previous section. We find this to be a striking result as these 250 RNA polymerase
493 molecules are responsible for the transcription of the ≈ 4000 protein coding genes that are not
494 ribosome associated.

495 tRNA

496 The final class of RNA molecules worthy of quantitative consideration is the the pool of tRNAs
497 used during translation to map codon sequence to amino acid identity. Unlike mRNA or rRNA,
498 each individual tRNA is remarkably short, ranging from 70 to 95 nucleotides each (BNID: 109645;
499 102340, *Milo et al. (2010)*). What they lack in length, they make up for in abundance. There are
500 many measurements of the size of the *E. coli* tRNA pool, ranging from $\approx 6 \times 10^4$ (BNID:105280, *Milo*
501 *et al. (2010)*) to $\approx 4 \times 10^5$ (BNID: 108611). To test tRNA synthesis as a possible growth-rate limiting
502 stage, we will err towards a higher abundance of $\approx 4 \times 10^5$ per cell. Combining the abundance and
503 tRNA length measurements, we make the estimate that $\approx 5 \times 10^7$ nucleotides are sequestered in
504 tRNA per cell. Unlike mRNA, tRNA is remarkably stable with typical lifetimes *in vivo* on the order of
505 ≈ 48 hours (*Abelson et al., 1974; Svenningsen et al., 2017*) – well beyond the timescale of division.
506 Once again using our rule-of-thumb for the rate of transcription to be 40 nucleotides per second
507 and assuming a division time of ≈ 5000 seconds, we arrive at an estimate of ≈ 150 RNA polymerases
508 to synthesize enough tRNA. This requirement pales in comparison to the number of polymerases
509 needed to generate the rRNA and mRNA pools and can be neglected as a significant transcriptional

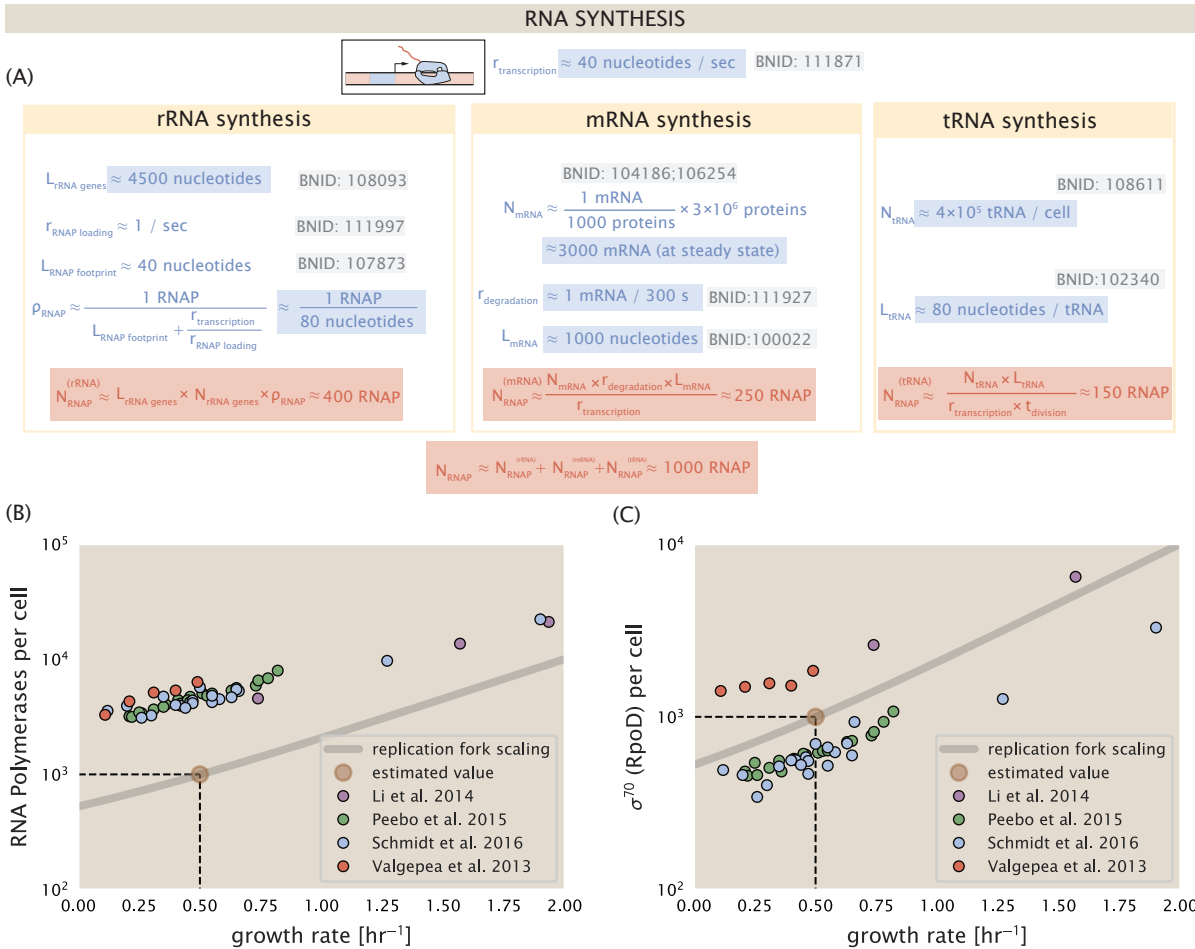


Figure 7. Estimation of the RNA polymerase demand and comparison with experimental data. (A)

Estimations for the number of RNA polymerase needed to synthesize sufficient quantities of rRNA, mRNA, and tRNA from left to right, respectively. Bionumber Identifiers (BNIDs) are provided for key quantities used in the estimates. (B) The RNA polymerase core enzyme copy number as a function of growth rate. Colored points correspond to the average number RNA polymerase core enzymes that could be formed given a subunit stoichiometry of $[RpoA]_2[RpoC][RpoB]$. (C) The abundance of σ^{70} as a function of growth rate. Estimated value for the number of RNAP is shown in (B) and (C) as a translucent brown point at a growth rate of 0.5 hr^{-1} .

510 burden.

511 RNA Polymerase and σ -factor Abundance

512 These estimates, summarized in **Figure 7 (A)**, reveal that synthesis of rRNA and mRNA are the domi-
513 nant RNA species synthesized by RNA polymerase, suggesting the need for ≈ 700 RNA polymerases
514 per cell. As is revealed in **Figure 7 (B)**, this estimate is about an order of magnitude below the ob-
515 served number of RNA polymerase complexes per cell ($\approx 5000 - 7000$). The disagreement between
516 the estimated number of RNA polymerases and these observations are at least consistent with
517 recent literature revealing that $\approx 80\%$ of RNA polymerases in *E. coli* are not transcriptionally active
518 (*Patrick et al., 2015*). Our estimate ignores the possibility that some fraction is only nonspecifically
519 bound to DNA, as well as the obstacles that RNA polymerase and DNA polymerase present for each
520 other as they move along the DNA (*Finkelstein and Greene, 2013*).

521 In addition, it is also vital to consider the role of σ -factors which help RNA polymerase identify
522 and bind to transcriptional start sites (*Browning and Busby, 2016*). Here we consider σ^{70} (RpoD)
523 which is the dominant "general-purpose" σ -factor in *E. coli*. While initially thought of as being solely

involved in transcriptional initiation, the past two decades of single-molecule work has revealed a more multipurpose role for σ^{70} including facilitating transcriptional elongation (*Kapanidis et al., 2005; Goldman et al., 2015; Perdue and Roberts, 2011; Mooney and Landick, 2003; Mooney et al., 2005*). **Figure 7** (B) is suggestive of such a role as the number of σ^{70} proteins per cell is in close agreement with our estimate of the number of transcriptional complexes needed.

These estimates provide insight as to the observed magnitude of both RNA polymerase and the σ -70 factor. As we have done in the previous sections, and described in the supplemental information, we can generalize these estimates across a wide range of growth rates (grey line in **Figure 7(B)**). While there remains some disagreement in the magnitude of the copy number, this estimate appears to very adequately describe the growth rate dependence of these complexes. Furthermore, these findings illustrate that transcription cannot be the rate limiting step in bacterial division. **Figure 7** (A) reveals that the availability of RNA polymerase is not a limiting factor for cell division as the cell always has an apparent \sim 10-fold excess than needed. Furthermore, if more transcriptional activity was needed to satisfy the cellular requirements, more σ^{70} -factors could be expressed to utilize a larger fraction of the RNA polymerase pool.

539 Translation and ribosomal synthesis

540 Lastly, we turn our attention to the process of synthesizing new proteins, translation. This process
 541 stands as a good candidate for potentially limiting growth since the synthesis of new proteins relies
 542 on the generation of ribosomes, themselves proteinaceous molecules. As we will see in the coming
 543 sections of this work, this poses a "chicken-or-the-egg" problem where the synthesis of ribosomes
 544 requires ribosomes in the first place.

545 We will begin our exploration of protein translation in the same spirit as we have in previous sections – we will draw order-of-magnitude estimates based on our intuition and available literature,
 546 and then compare these estimates to the observed data. In doing so, we will estimate both the
 547 absolute number of ribosomes necessary for replication of the proteome as well as the synthesis
 548 of amino-acyl tRNAs. From there we consider the limitations on ribosomal synthesis in light of our
 549 estimates on both the synthesis of ribosomal proteins and our earlier results on rRNA synthesis.

551 tRNA synthetases

552 We begin by first estimating the number of tRNA synthetases in *E. coli* needed to convert free amino-
 553 acids to polypeptide chains. At a modest growth rate of \approx 5000 s, *E. coli* has roughly 3×10^6 proteins
 554 per cell (BNID: 115702; *Milo et al. (2010)*). Assuming that the typical protein is on the order of \approx
 555 300 amino acids in length (BNID: 100017; *Milo et al. (2010)*), we can estimate that a total of $\approx 10^9$
 556 amino acids are stitched together by peptide bonds.

557 How many tRNAs are needed to facilitate this remarkable number of amino acid delivery events
 558 to the translating ribosomes? It is important to note that tRNAs are recycled after they've passed
 559 through the ribosome and can be recharged with a new amino acid, ready for another round of
 560 peptide bond formation. While some *in vitro* data exists on the turnover of tRNA in *E. coli* for
 561 different amino acids, we can make a reasonable estimate by comparing the number of amino
 562 acids to be polymerized to cell division time. Using our stopwatch of 5000 s and 10^9 amino acids,
 563 we arrive at a requirement of $\approx 2 \times 10^5$ tRNA molecules. This estimate is in line with experimental
 564 measurements of $\approx 3 \times 10^5$ per cell (BNID: 108611, *Milo et al. (2010)*), suggesting we are on the
 565 right track.

566 There are many processes which go into synthesizing a tRNA and ligating it with the appropriate
 567 amino acids. As we covered in the previous section, there appear to be more than enough RNA
 568 polymerases per cell to synthesize the needed pool of tRNAs. Without considering the many ways
 569 in which amino acids can be scavenged or synthesized *de novo*, we can explore ligation the as a
 570 potential rate limiting step. The enzymes which link the correct amino acid to the tRNA, known as
 571 tRNA synthetases or tRNA ligases, are incredible in their proofreading of substrates with the incor-
 572 rect amino acid being ligated once out of every 10^4 to 10^5 times (BNID: 103469, *Milo et al. (2010)*).

573 This is due in part to the consumption of energy as well as a multi-step pathway to ligation. While
 574 the rate at which tRNA is ligated is highly dependent on the identity of the amino acid, it is reason-
 575 able to state that the typical tRNA synthetase has charging rate of ≈ 20 AA per tRNA synthetase per
 576 second (BNID: 105279, *Milo et al. (2010)*).

577 Combining these estimates together, as shown schematically in *Figure 8(A)*, yields an estimate
 578 of $\approx 10^4$ tRNA synthetases per cell with a division time of 5000 s. This point estimate is in very close
 579 agreement with the observed number of synthetases (the sum of all 20 tRNA synthetases in *E. coli*).
 580 This estimation strategy seems to adequately describe the observed growth rate dependence of
 581 the tRNA synthetase copy number (shown as the grey line in *Figure 8(B)*), suggesting that the copy
 582 number scales with the cell volume.

583 In total, the estimated and observed $\approx 10^4$ tRNA synthetases occupy only a meager fraction of
 584 the total cell proteome, around 0.5% by abundance. It is reasonable to assume that if tRNA charg-
 585 ing was a rate limiting process, cells would be able to increase their growth rate by devoting more
 586 cellular resources to making more tRNA synthases. As the synthesis of tRNAs and the correspond-
 587 ing charging can be highly parallelized, we can argue that tRNA charging is not a rate limiting step
 588 in cell division, at least for the growth conditions explored in this work.

589 Protein synthesis

590 With the number of tRNA synthetases accounted for, we now consider the abundance of the pro-
 591 tein synthesis machines themselves, ribosomes. Ribosomes are enormous protein/rRNA com-
 592 plexes that facilitate the peptide bond formation between amino acids in the correct sequence
 593 as defined by the coding mRNA. Before we examine the synthesis of the ribosome proteins and
 594 the limits that may place on the observed bacterial growth rates, let's consider replication of the
 595 cellular proteome.

596 As described in the previous section, an *E. coli* cell consisting of $\approx 3 \times 10^6$ proteins will have
 597 on the order $\approx 10^9$ peptide bonds per proteome. While the rate at which ribosomes translates is
 598 well known to have a growth rate dependence *Dai et al. (2018)* and is a topic which we discuss in
 599 detail in the coming sections. However, for the purposes of our order-of-magnitude estimate, we
 600 can make the approximation that translation occurs at a rate of ≈ 15 amino acids per second per
 601 ribosome (BNID: 100233, *Milo et al. (2010)*). Under this approximation and assuming a division
 602 time of 5000 s, we can arrive at an estimate of $\approx 10^4$ ribosomes are needed to replicate the cellular
 603 proteome, shown in *Figure 8(B)*. This point estimate, while glossing over important details such
 604 as chromosome copy number and growth-rate dependent translation rates, proves to be notably
 605 accurate when compared to the experimental observations (*Figure 8(B)*).

606 Translation as a growth-rate limiting step

607 Thus far, the general back-of-the-envelope estimates have been reasonably successful in explain-
 608 ing what sets the scale of absolute protein copy number. A recurring theme that has arisen is the
 609 ability of cells to parallelize their biosynthesis tasks. For example, while DNA replication speed-limit
 610 is ≈ 40 minutes to replicate a genome, cells can divide faster than this by initiating more than one
 611 round of replication per doubling. However, as we will see, parallelization is not possible when it
 612 comes to the translation of ribosomal proteins (*Figure 9(A)*). Thus, it is plausible that translation
 613 may be a key factor in determining the cellular growth rate.

614 To gain some intuition into how translation can set the speed of bacterial growth, we again
 615 consider the total number of peptide bonds that must be synthesized, which we denote as N_{AA} .
 616 Noting that cells grow exponentially in time (*Godin et al., 2010*), we can compute the number of
 617 amino acids to be polymerized as

$$N_{AA}\lambda = r_t R, \quad (1)$$

618 where λ is the cell growth rate in s^{-1} , r_t is the maximum translation rate in $AA \cdot s^{-1}$, and R is the
 619 average ribosome copy number per cell. Knowing the number of peptide bonds to be formed

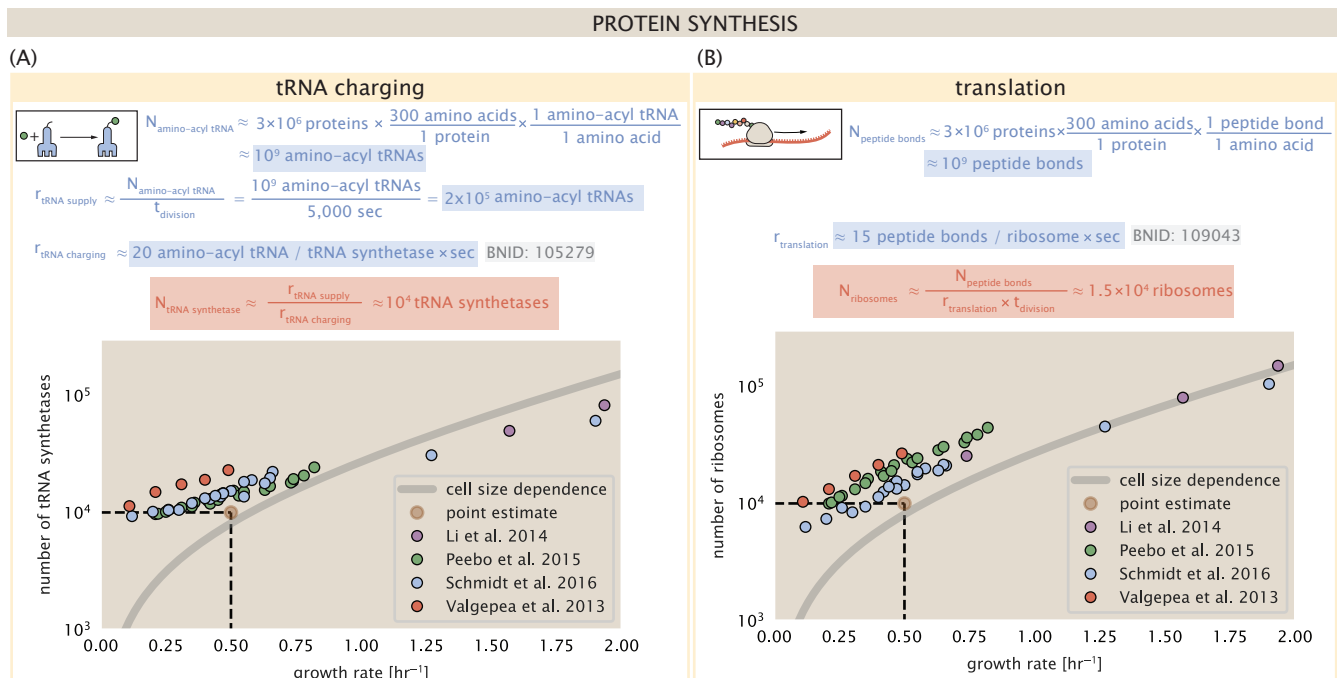


Figure 8. Estimation of the required tRNA synthetases and ribosomes. (A) Estimation for the number of tRNA synthetases that will supply the required amino acid demand. The sum of all tRNA synthetases copy numbers are plotted as a function of growth rate ([ArgS], [CysS], [GlnS], [Glx], [IleS], [LeuS], [ValS], [AlaS]₂, [AsnS]₂, [AspS]₂, [TyrS]₂, [TrpS]₂, [ThrS]₂, [SerS]₂, [ProS]₂, [PheS]₂[PheT]₂, [MetG]₂, [LysS]₂, [HisS]₂, [GlyS]₂[GlyQ]₂). (B) Estimation of the number of ribosomes required to synthesize 10⁹ peptide bonds with an elongation rate of 15 peptide bonds per second. The average abundance of ribosomes is plotted as a function of growth rate. Our estimated values are shown for a growth rate of 0.5 hr⁻¹. Grey lines correspond to the estimated complex abundance calculated at different growth rates. See Supplemental Information XX for a more detail description of this calculation.

620 permits us to compute the translation-limited growth rate as

$$\lambda_{\text{translation-limited}} = \frac{r_t R}{N_{\text{AA}}}. \quad (2)$$

621 Alternatively, since N_{AA} is related to the total protein mass through the molecular weight of
 622 each protein, we can also consider the growth rate in terms of the fraction of the total proteome
 623 mass that is dedicated to ribosomal protein mass. By making the approximation that an average
 624 amino acid has a molecular weight of 110 Da (BNID: 104877, *Milo et al. (2010)*), we can approximate
 625 $R/N_{\text{AA}} \approx \Phi_R/L_R$, where Φ_R is the ribosomal mass fraction and L_R is the total length in amino acids
 626 that make up a ribosome. The translation-limited growth rate can then be written in the form

$$\lambda_{\text{translation-limited}} \approx \frac{r_t}{L_R} \Phi_R. \quad (3)$$

627 This is plotted as a function of ribosomal fraction Φ_R in *Figure 9(B)*, where we take $L_R \approx 7500$ AA,
 628 corresponding to the length in amino acids for all ribosomal subunits of the 50S and 30S complex
 629 (BNID: 101175, *(Milo et al., 2010)*).

630 The growth rate defined by *Equation 3* reflects mass-balance under steady-state growth and
 631 has long provided a rationalization of the apparent linear increase in *E. coli*'s ribosomal content
 632 as a function of growth rate (*Maaløe, 1979; Scott et al., 2010*). We note that there is a maximum
 633 growth rate of $\lambda \approx 8 \text{ hr}^{-1}$, or a doubling time just under 6 minutes (*Figure 9(B)*, dashed line). This
 634 represents an inherent speed limit due to the need for the cell to double its entire ribosomal mass.
 635 Interestingly, this limit is independent of the absolute number of ribosomes and is simply given by
 636 the time to translate an entire ribosome, L_R/r_t . As shown in *Figure 9(A)*, we can reconcile this with
 637 the observation that in order to double the average number of ribosomes, each ribosome must
 638 produce a second ribosome and cannot be parallelized.

639 Earlier, we considered rRNA synthesis (see Section **RNA Synthesis**), finding that, when the rRNA
 640 operons are maximally loaded with RNA polymerase, the cell can produce ≈ 1 functional rRNA unit
 641 per second per operon. In *Figure 9(C)*, we show the maximum number of ribosomes that could
 642 be made as a function of growth rate given this rRNA production rule-of-thumb. While each *E.*
 643 *coli* genome has 7 copies of the rRNA operon (BNID: 107866, *Milo et al. (2010)*), parallelization
 644 of DNA synthesis by firing multiple rounds of replication at a time can drastically the effective
 645 number of rRNA operons. The blue curve in ??, we assume that the effective number of rRNA
 646 operons increases in proportion to the number of origins of replication (# ori) (solid blue line;
 647 with the calculation of (# ori) described in the next section). Although we expect this value to
 648 drastically overestimate rRNA abundance at slower growth rates ($\lambda < 0.5 \text{ hr}^{-1}$), it provides a useful
 649 reference when considered along with the proteomic measurements that are also plotted. For
 650 growth rates above about 1 hr^{-1} , we find that cells will need to transcribe rRNA near their maximal
 651 rate. The dashed blue curve in *Figure 9(C)* shows the maximal number of functional rRNA units
 652 that could be synthesized from a single genome (ignoring the chromosome replication speed limit
 653 of ≈ 40 minutes per genome). The convergence between the maximum rRNA production with
 654 parallelization and the experimentally measured ribosome copy number (points in *Figure 9(C)*), as
 655 well as the observation cells are rarely reported to grow faster than 2 hr^{-1} (*Bremer and Dennis,*
 656 *2008*), suggests rRNA synthesis represents the rate limiting step in cell division for this strain of *E.*
 657 *coli*.

658 Relationship between cell size and growth rate.

659 With the observation that ribosomes set an inherent upper limit on growth rate, through both rRNA
 660 synthesis and the additional dependence on ribosomal fraction, it is also plausible that ribosomes
 661 may play a more dominant role in setting growth rate across other growth conditions. With a rich
 662 proteomic data set across a wide array of conditions, and in light of a number of recent experi-
 663 mental observations, we find that cells also appear to tune their ribosomal abundance as a means
 664 to maximize growth even in poor nutrient conditions. This has important consequences on the

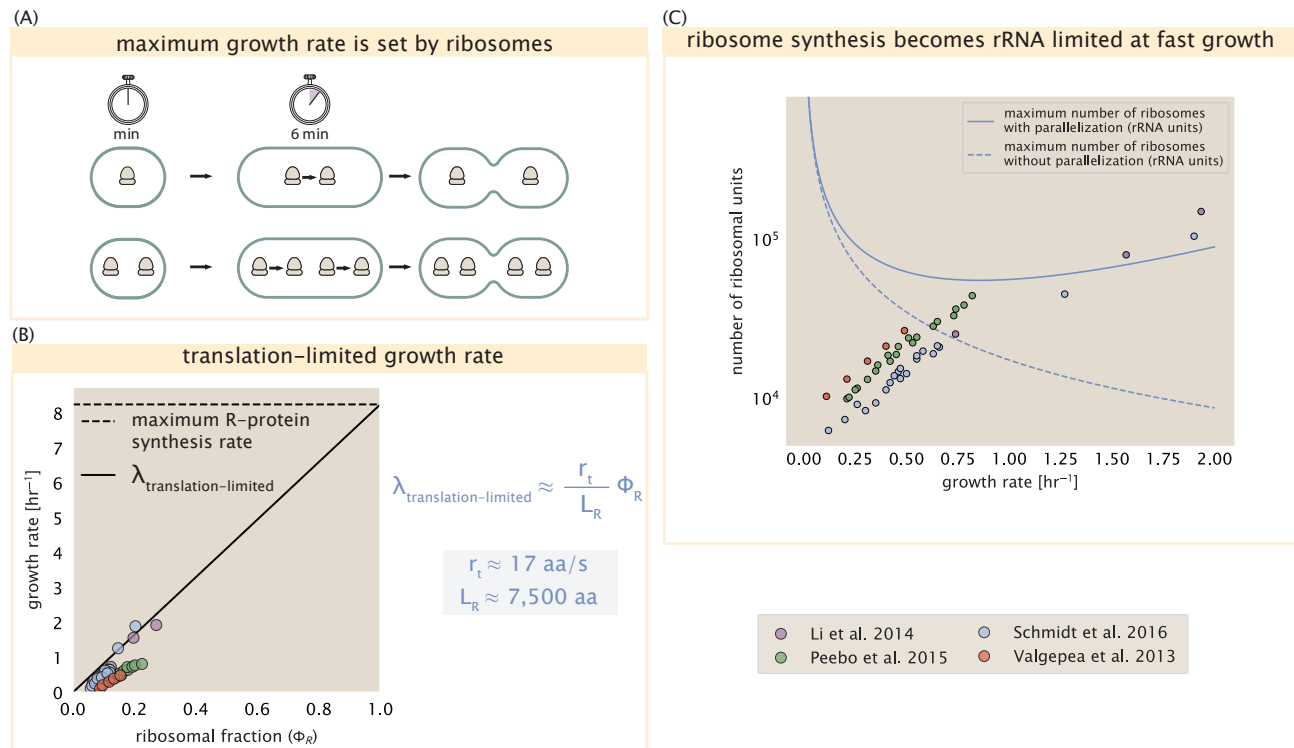


Figure 9. Translation-limited growth rate. (A) Here we consider the translation-limited growth rate as a function of ribosomal fraction. By mass balance, the time required to double the entire proteome (N_{AA} / r_t) sets the translation-limited growth rate, $\lambda_{\text{translation-limited}}$. Here N_{AA} is effectively the number of peptide bonds that must be translated, r_t is the translation elongation rate, and R is the number of ribosomes. This can also be re-written in terms of the ribosomal mass fraction $\Phi_R = m_R / m_{\text{protein}}$, where m_R is the total ribosomal mass and m_{protein} is the mass of all proteins in the cell. L_R refers to the summed length of the ribosome in amino acids. $\lambda_{\text{translation-limited}}$ is plotted as a function of Φ_R (solid line). (B) The dashed line in part (A) identifies a maximum growth rate that is set by the ribosome. Specifically, this growth rate corresponds to the time required to translate an entire ribosome, L_R / r_t . This is a result that is independent of the number of ribosomes in the cell as shown schematically here. (C) Maximum number of rRNA units that can be synthesized as a function of growth rate. Solid curve corresponds to the rRNA copy number calculated by multiplying the number of rRNA operons by the estimated number of (# ori) at each growth rate. The quantity (# ori) was calculated using Equation 4 and the measurements from Si et al. (2017) that are plotted in Figure 10(A). Dashed line show that maximal number of functional rRNA units produced from a single chromosome without parallelization.

665 relationship with cell size and maintenance of steady-state growth. In the coming section and the
666 remainder of the text, we consider these further beginning with cell size.

667 The relationship between cell size and growth rate has long been of interest in the study of
668 bacterial physiology, particularly following the now six decade-old observation that cell volume
669 appears to increase exponentially with growth rate; known as Schaechter's growth law (*Schaechter*
670 *et al.*, 1958; *Taheri-Araghi et al.*, 2015). Wild-type *E. coli* growing at relatively fast growth rates
671 exhibit a remarkably constant cell cycle time t_{cyc} (referring to the C and D periods of DNA replication
672 and cell division, respectively), as shown in **Figure 10(A)** for the data reproduced from *Si et al.* (2017).
673 With a constant cell cycle time, the exponential scaling in size has long been considered a direct
674 consequence of cells initiating replication at a constant volume per origin. However, the particular
675 mechanism that governs this relationship, and even the question of whether the change in average
676 cell size is truly exponential have remained under debate (*Si et al.*, 2017; *Harris and Theriot*, 2018).

677 Since protein accounts for more than half of cellular dry mass (BNID: 104954, *Milo et al.* (2010);
678 *Bremer and Dennis* (2008); *Basan et al.* (2015)), cell size will vary in proportion to how much protein
679 is synthesized over the cell cycle. Through our estimates in the sections on the central dogma, it is
680 apparent that the processes of transcription (i.e. synthesis of mRNA) and translation are unlikely
681 limiting steps in doubling the cell mass. In both cases, there is an overabundance of the requisite
682 protein complexes (DNA and RNA polymerase, respectively) and there are mechanisms by which
683 these synthesis processes can be parallelized. Therefore, the total protein mass is determined by
684 $r_i \times R$ and the doubling time τ . The relationship between cell size and growth rate, however, will
685 depend only on how the cell scales its ribosomal fraction Φ_R , as highlighted by **Equation 3**.

686 Ribosomal abundance defines exponential scaling between cell size and growth rate
687 A naïve strategy to increase growth rate given the constraint prescribed by **Equation 3**, would be
688 to simply generate more ribosomes. In reality, large swaths of the proteome increases in absolute
689 abundance at faster growth (Supplemental Figure X). Substantial empirical evidence has revealed
690 a linear scaling between cell size (volume) and the number of chromosomal origins of replication,
691 $\langle \# \text{ ori} \rangle$, which is robust to a remarkable array of perturbations (*Si et al.*, 2017). The number of
692 origins $\langle \# \text{ ori} \rangle$ is determined by how often replication must be initiated per cell doubling to maintain
693 steady-state growth and can be quantified via

$$\langle \# \text{ ori} \rangle \approx 2^{\tau_{cyc}/\tau}, \quad (4)$$

694 where τ is the doubling time. In **Figure 10(A)**, we show the measurements of *Si et al.* (2017) for
695 wild-type *E. coli* cells in nutrient-limit growth regimes. Using this data, we estimated $\langle \# \text{ ori} \rangle$ for each
696 condition in the amalgamated proteomic datasets. With rRNA otherwise becoming rate limited at
697 fast growth, this strategy allows for a roughly linear increase in ribosomes copy number with $\langle \#$
698 $\text{ori} \rangle$ as shown in **Figure 10(B)** for the proteomic data.

699 It is notable that in *E. coli*, the majority of ribosomal proteins and rRNA operons are found
700 closer to the origin of replication. Since multiple rounds of DNA initiation will effectively skew gene
701 dosage in favor of genes near the origin (*Scholz et al.*, 2019), it suggests that an increase in $\langle \# \text{ ori} \rangle$
702 is a means to skew the ribosomal fraction of the proteome, Φ_R . In **Figure 10(D)** we show that this
703 skew in gene dosage is reflected in the composition of the proteome via a running boxcar average
704 (500 kbp window) of protein copy number as a function of each gene's transcriptional start site
705 (**Figure 10(D)**). While the protein copy numbers of individual proteins can vary substantially across
706 the entire chromosome, we nonetheless observe a bias in expression across the chromosome
707 under fast growth conditions (dark blue lines) relative to slow growth (yellow lines). The dramatic
708 change in protein copy number near the origin is largely due to the increase in ribosomal protein
709 expression. This trend is in contrast to slower growth conditions (yellow) where the average copy
710 number is much more uniform across the length of the chromosome.

711 This result provides important evidence that although total protein content scales with $\langle \# \text{ ori} \rangle$, it
712 is also the bias in gene dosage for genes closer to the origin that change the proteomic composition

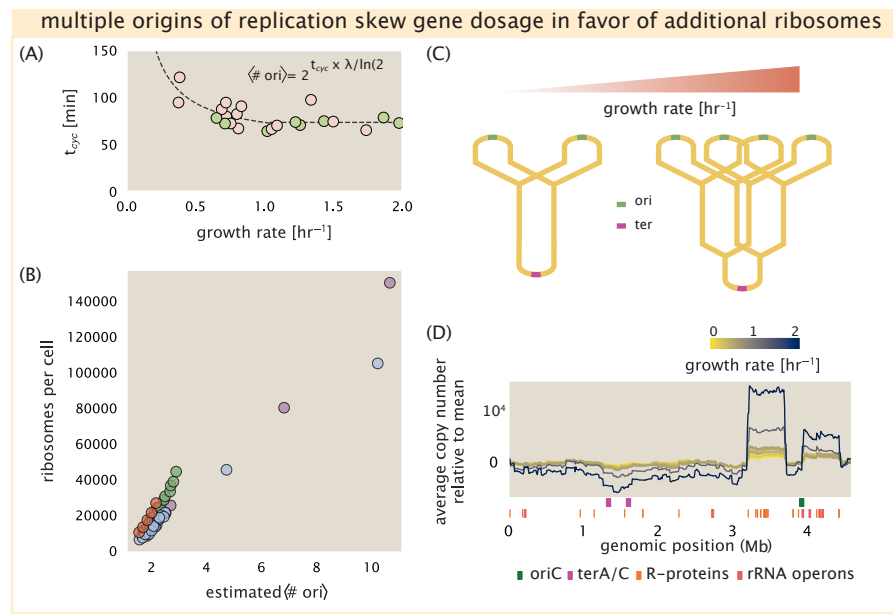


Figure 10. Multiple replication forks skew gene dosage and ribosomal content. (A) Experimental data from Si *et al.* (2017). Dashed line shows fit to the data, which were used to estimate $\langle \# \text{ori} \rangle$. t_{cyc} was assumed to vary in proportion to τ for doubling times great than 40 minutes, and then reach a minimum value of [fill in] minutes below this (see Supplemental Appendix X for additional details). Red data points correspond to measurements in strain MG1655, while light green points are for strain NCM3722. (B) Plot of the ribosome copy number estimated from the proteomic data against the estimated $\langle \# \text{ori} \rangle$ [NB: change to total protein abundance?]. (C) Schematic shows the expected increase in replication forks (or number of ori regions) as *E. coli* cells grow faster. (D) A running boxcar average of protein copy number is calculated for each each growth condition considered by (Schmidt *et al.*, 2016). A 0.5 Mb averaging window was used. Protein copy numbers are reported relative to their condition-specific means in order to center all data sets.

and allows an increase in the ribosomal fraction Φ_R at fast growth. For *E. coli*, we can then view the increase in ribosomal fraction Φ_R (and therefore, λ) as requiring a geometric increase in total protein abundance that is proportional to (# ori). This leads to an exponential increase in total protein mass (and cell size) as long as all ribosomes R are actively translating protein during cell doubling.

While our analysis suggests that it is the need to increase the absolute number of ribosomes that sets an exponential scaling in cell size, this relationship is likely to falter at slow growth rates (below $\lambda \approx 0.5 \text{ hr}^{-1}$). In this regime, ribosome abundance R no longer reflects the cell's protein synthesis capacity (Dai et al., 2016), so far taken to be $r_t \times R$. Additional regulatory control through the small-molecule alarmones such as guanosine pentaphosphate [(p)ppGpp] reduces the fraction of actively translating ribosomes at slow growth and yields a translational capacity below $r_t \times R$. This is why Si et al. (2017) found that it was the change in active ribosomal fraction, and not ribosomal fraction alone, that was most consistent with an exponential change in cell size. The specific relationship between cell size and growth rate however becomes harder to define because cells no longer need multiple rounds of DNA replication to make enough rRNA, and no longer need to increase their total protein mass in order to tune protein synthesis. Our collated proteomic data, however, contain several assumptions that relate total protein abundance to growth rates and this prevents us from making precise predictions about how cell size and absolute protein abundance vary at slow growth (Supplemental X). Nevertheless, we find no evidence that cells decrease their size to the minimal value expected from an exponential function with a constant exponent fit to cell sizes with moderate to fast growth rates (Basan et al., 2015; JL et al., 2016; Si et al., 2019), suggesting at least a modified scaling between size and growth rate in these poorer nutrient conditions.

736 Growth in poor nutrient conditions.

737 How do cells regulate protein synthesis when amino acids become limiting, meaning that con-
 738 sumption exceeds the rate of synthesis? In the slowest growth conditions, we find a minimum
 739 ribosomal mass fraction of $\Phi_R \approx 0.06$ and of order 10^4 ribosomes per cell. Without the additional
 740 regulatory control noted above, there would be a point where this imbalance would occur if all
 741 ribosomes were actively translating (Figure 11). Such a scenario would prevent continuous growth,
 742 and indeed for (p)ppGpp null strains, cells only grow in minimal media if additional amino acid
 743 supplements are present. In contrast, wild-type *E. coli* maintain a relatively high elongation rate
 744 even in stationary phase ($\approx 8 \text{ AA/s}$, (Dai et al., 2016, 2018)).

745 To better understand how regulation of ribosomes influence growth rate at slow growth, we
 746 consider a coarse-grained model that relates elongation rate to a limiting supply of amino acids,
 747 which for simplicity we treat as a single, effective rate-limiting species $[AA]_{eff}$. Under such a sce-
 748 nario, the elongation rate r_t can be described as depending on the maximum elongation rate ($r_t^{max} \approx$
 749 17.1 AA/s , (Dai et al., 2016, 2018)), an effective binding constant K_D between the pool of amino acids
 750 and their amino-acyl tRNAs, and the limiting amino acid concentration $[AA]_{eff}$,

$$r_t = r_t^{max} \cdot \frac{1}{1 + K_D/[AA]_{eff}}. \quad (5)$$

751 For cells growing in minimal medium supplemented with glucose, the amino acid concentration is
 752 of order 100 mM (BNID: 110093, (Milo et al., 2010; Bennett et al., 2009)). To estimate K_D , we note
 753 that for a growth rate of about 0.6 hr^{-1} Dai et al. (2016) measured an elongation rate of about 12.5
 754 $\text{AA} \cdot \text{s}^{-1}$, yielding $K_D \approx 40 \text{ mM}$. The maintenance of this amino acid pool $[AA]_{eff}$ will depend on the
 755 difference between the synthesis/supply rate of amino acids r_{AA} and consumption by ribosomes
 756 $r_t \times R \times f_a$, where we use f_a to account for the possible reduction of actively translating ribosomes
 757 (see Supplemental Appendix XX for further details on this model).

758 In Figure 11(B), we show the relationship between the growth rate and elongation rate as a
 759 function of the number of actively translating ribosomes. Here, growth rate is now determined by

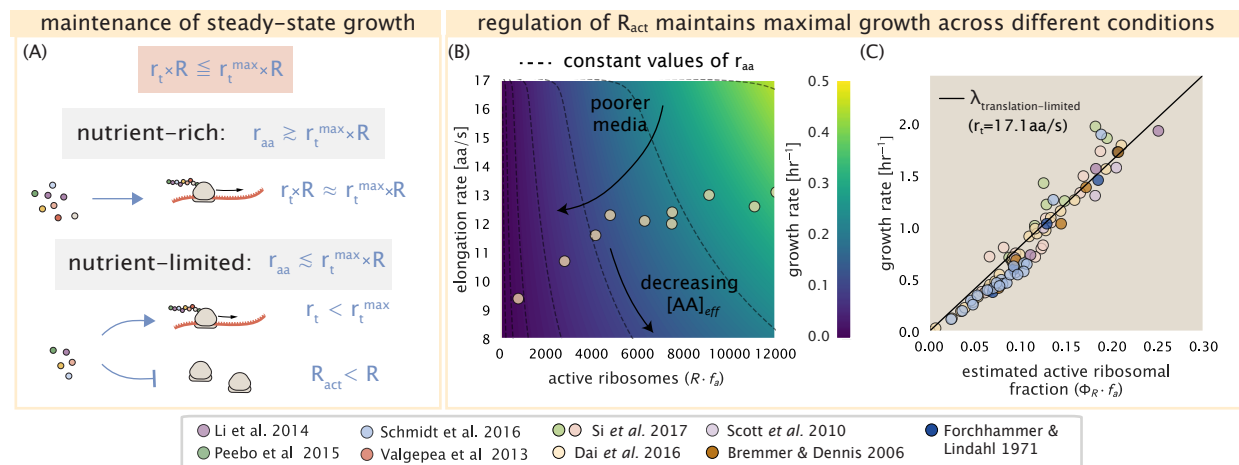


Figure 11. *E. coli* must regulate ribosomal activity in limiting nutrient conditions. (A) Schematic showing translation-specific requirements for maintenance of steady-state growth. In a nutrient rich environment, amino acid supply r_{aa} is sufficiently in excess of the demand by ribosomes translating at their maximal rate. In poorer nutrient conditions, reduced amino acid supply r_{aa} will decrease the rate of elongation. In a regime where r_{aa} is less than $r_t R$, the number of actively translating ribosomes will need to be reduced in order to maintain steady-state growth. (B) Translation elongation rate is plotted as a function of the number of actively translating ribosomes $R f_a$. Dashed lines correspond to a range of amino acid synthesis rates r_{aa} , from 10^3 to 10^6 . Growth rates are calculated according to Equation 1, assuming a constant ribosomal fraction of 8 percent. See appendix XX for additional details. (C) Experimental data from (Dai et al., 2016) are used to estimate the fraction of actively translating ribosomes. The solid line represents the translation-limited growth rate for ribosomes elongating at 17.1 AA/s.

760 the active ribosomal fraction via

$$\lambda_{\text{translation-limited}} \approx \frac{r_t}{L_R} \Phi_R f_a. \quad (6)$$

761 If we consider constant values of amino acid synthesis rate r_{AA} (dashed lines) to reflect the available
 762 parameter space for a specific growth condition, the fastest growth rates result from maximization
 763 of the fraction of actively translating ribosomes. When we consider the experimental measure-
 764 ments from **Dai et al. (2018)** (yellow circles), reflecting growth in different nutrient conditions, we
 765 see that although $R \times f_a$ is reduced in poorer nutrient conditions, it is reduced in a manner such that
 766 $[AA]_{eff}$ is relatively constant. Given our estimate $K_D \approx 40$ mM, we would only expect a decrease
 767 from 100 mM to about 35 mM in the slowest growth conditions. While experimental data is scarce,
 768 data from **Bennett et al. (2009)** show that amino acid concentrations only decrease to about 60
 769 mM for cells grown in minimal media supplemented with acetate ($\lambda \approx 0.3 \text{ hr}^{-1}$ in our proteomic
 770 data) (**Bennett et al., 2009**), qualitatively consistent with our expectations. One explanation for the
 771 experimental data is that the active fraction of the ribosome pool is regulated in order to maintain
 772 a sufficient supply of amino acids for growth. Any further increase in $R \times f_a$ at constant r_{AA} would
 773 otherwise be associated with an additional drop in cellular amino acid concentration.

774 *E. coli* maximizes its steady-state growth rate by tuning both ribosomal content and trans-
 775 lation activity.

776 Using the active fraction f_a measurements across a broad range of nutrient-limited growth condi-
 777 tions from the work of **Dai et al. (2016)**, we furthermore estimated the active fraction of ribosomal
 778 protein across the collated proteomic datasets (Figure 11(C)). Importantly, we note that across all
 779 growth conditions considered, cells appear to maintain a growth rate consistent with **Equation 3**
 780 with an elongation rate of $r_t \approx 17.1 \text{ AA/s}$. While somewhat counter intuitive, given that ribosomes
 781 translate at almost half this rate in the poorest of growth conditions, steady-state growth rates can

782 be achieved over such a broad range of conditions because cells have evolved a means to tune
783 $r_t \times R \times f_a$.

784 It has recently been shown that growth in a (p)ppGpp null strain abolishes both the the growth-
785 dependent changes in gene dosage and scaling in cell size. Instead, cells always exhibited a higher
786 gene dosage near near the origin of replication, irrespective of growth rate, and a cell size more
787 consistent with a fast growth state where (p)ppGpp levels are low (*Fernández-Coll et al., 2020*) and
788 ribosomal fraction is high (*Zhu and Dai, 2019*). This raises the possibility that the action of (p)ppGpp
789 is also mediating growth control and size scaling over the entire range of growth conditions. Specif-
790 ically, as nutrient conditions worsen, (p)ppGpp helps decrease multiple rounds of DNA replication
791 per cell doubling which effectively decreases both R and the total cell size *and* in sufficiently poor
792 growth conditions mitigates translation activity according to nutrient availability.

793 References

- 794 Abelson, H., Johnson, L., Penman, S., and Green, H. (1974). Changes in RNA in relation to growth of the fibroblast:
 795 II. The lifetime of mRNA, rRNA, and tRNA in resting and growing cells. *Cell*, 1(4):161–165.
- 796 Aidelberg, G., Towbin, B. D., Rothschild, D., Dekel, E., Bren, A., and Alon, U. (2014). Hierarchy of non-glucose
 797 sugars in *Escherichia coli*. *BMC Systems Biology*, 8(1):133.
- 798 Antonenko, Y. N., Pohl, P., and Denisov, G. A. (1997). Permeation of ammonia across bilayer lipid membranes
 799 studied by ammonium ion selective microelectrodes. *Biophysical Journal*, 72(5):2187–2195.
- 800 Ashburner, M., Ball, C. A., Blake, J. A., Botstein, D., Butler, H., Cherry, J. M., Davis, A. P., Dolinski, K., Dwight, S. S.,
 801 Eppig, J. T., Harris, M. A., Hill, D. P., Ireson-Tarver, L., Kasarskis, A., Lewis, S., Matese, J. C., Richardson, J. E.,
 802 Ringwald, M., Rubin, G. M., and Sherlock, G. (2000). Gene Ontology: tool for the unification of biology. *Nature Genetics*, 25(1):25–29.
- 803 Ason, B., Bertram, J. G., Hingorani, M. M., Beechem, J. M., O'Donnell, M., Goodman, M. F., and Bloom, L. B.
 804 (2000). A Model for *Escherichia coli* DNA Polymerase III Holoenzyme Assembly at Primer/Template Ends:
 805 DNA Triggers A Change In Binding Specificity of the γ Complex Clamp Loader. *Journal of Biological Chemistry*,
 806 275(4):3006–3015.
- 807 Assentoft, M., Kaptan, S., Schneider, H.-P., Deitmer, J. W., de Groot, B. L., and MacAulay, N. (2016). Aquaporin 4
 808 as a NH₃ Channel. *Journal of Biological Chemistry*, 291(36):19184–19195.
- 809 Basan, M., Zhu, M., Dai, X., Warren, M., Sévin, D., Wang, Y.-P., and Hwa, T. (2015). Inflating bacterial cells by
 810 increased protein synthesis. *Molecular Systems Biology*, 11(10):836.
- 811 Bauer, S. and Ziv, E. (1976). Dense growth of aerobic bacteria in a bench-scale fermentor. *Biotechnology and
 812 Bioengineering*, 18(1):81–94. _eprint: <https://onlinelibrary.wiley.com/doi/10.1002/bit.260180107>.
- 813 Belliveau, N. M., Barnes, S. L., Ireland, W. T., Jones, D. L., Sweredoski, M. J., Moradian, A., Hess, S., Kinney, J. B.,
 814 and Phillips, R. (2018). Systematic approach for dissecting the molecular mechanisms of transcriptional
 815 regulation in bacteria. *Proceedings of the National Academy of Sciences*, 115(21):E4796–E4805.
- 816 Bennett, B. D., Kimball, E. H., Gao, M., Osterhout, R., Van Dien, S. J., and Rabinowitz, J. D. (2009). Absolute
 817 metabolite concentrations and implied enzyme active site occupancy in *Escherichia coli*. *Nature Chemical
 818 Biology*, 5(8):593–599.
- 819 Birnbaum, L. S. and Kaplan, S. (1971). Localization of a Portion of the Ribosomal RNA Genes in *Escherichia coli*.
 820 *Proceedings of the National Academy of Sciences*, 68(5):925–929.
- 821 Booth, I. R., Mitchell, W. J., and Hamilton, W. A. (1979). Quantitative analysis of proton-linked transport systems.
 822 The lactose permease of *Escherichia coli*. *Biochemical Journal*, 182(3):687–696.
- 823 Bremer, H. and Dennis, P. P. (2008). Modulation of Chemical Composition and Other Parameters of the Cell at
 824 Different Exponential Growth Rates. *EcoSal Plus*, 3(1).
- 825 Browning, D. F. and Busby, S. J. W. (2016). Local and global regulation of transcription initiation in bacteria.
 826 *Nature Reviews Microbiology*, 14(10):638–650.
- 827 Cox, G. B., Newton, N. A., Gibson, F., Snoswell, A. M., and Hamilton, J. A. (1970). The function of ubiquinone in
 828 *Escherichia coli*. *Biochemical Journal*, 117(3):551–562.
- 829 Dai, X., Zhu, M., Warren, M., Balakrishnan, R., Okano, H., Williamson, J. R., Fredrick, K., and Hwa, T. (2018).
 830 Slowdown of Translational Elongation in *Escherichia coli* under Hyperosmotic Stress. - PubMed - NCBI. *mBio*,
 831 9(1):281.
- 832 Dai, X., Zhu, M., Warren, M., Balakrishnan, R., Patsalo, V., Okano, H., Williamson, J. R., Fredrick, K., Wang, Y.-P.,
 833 and Hwa, T. (2016). Reduction of translating ribosomes enables *Escherichia coli* to maintain elongation rates
 834 during slow growth. *Nature Microbiology*, 2(2):16231.
- 835 Escalante, A., Salinas Cervantes, A., Gosset, G., and Bolívar, F. (2012). Current knowledge of the *Escherichia coli*
 836 phosphoenolpyruvate-carbohydrate phosphotransferase system: Peculiarities of regulation and impact on
 837 growth and product formation. *Applied Microbiology and Biotechnology*, 94(6):1483–1494.
- 838 Feist, A. M., Henry, C. S., Reed, J. L., Krummenacker, M., Joyce, A. R., Karp, P. D., Broadbelt, L. J., Hatzimanikatis,
 839 V., and Palsson, B. Ø. (2007). A genome-scale metabolic reconstruction for *Escherichia coli* K-12 MG1655 that
 840 accounts for 1260 ORFs and thermodynamic information. *Molecular Systems Biology*, 3(1):121.

- 842 Fernández-Coll, L., Maciąg-Dorszynska, M., Tailor, K., Vadia, S., Levin, P. A., Szalewska-Palasz, A., Cashel, M.,
 843 and Dunny, G. M. (2020). The Absence of (p)ppGpp Renders Initiation of *Escherichia coli* Chromosomal DNA
 844 Synthesis Independent of Growth Rates. *mBio*, 11(2):45.
- 845 Fijalkowska, I. J., Schaaper, R. M., and Jonczyk, P. (2012). DNA replication fidelity in *Escherichia coli*: A multi-DNA
 846 polymerase affair. *FEMS Microbiology Reviews*, 36(6):1105–1121.
- 847 Finkelstein, I. J. and Greene, E. C. (2013). Molecular Traffic Jams on DNA. *Annual Review of Biophysics*, 42(1):241–
 848 263.
- 849 Gama-Castro, S., Salgado, H., Santos-Zavaleta, A., Ledezma-Tejeida, D., Muñiz-Rascado, L., García-Sotelo, J. S.,
 850 Alquicira-Hernández, K., Martínez-Flores, I., Pannier, L., Castro-Mondragón, J. A., Medina-Rivera, A., Solano-
 851 Lira, H., Bonavides-Martínez, C., Pérez-Rueda, E., Alquicira-Hernández, S., Porrón-Sotelo, L., López-Fuentes,
 852 A., Hernández-Koutoucheva, A., Moral-Chávez, V. D., Rinaldi, F., and Collado-Vides, J. (2016). RegulonDB
 853 version 9.0: High-level integration of gene regulation, coexpression, motif clustering and beyond. *Nucleic
 854 Acids Research*, 44(D1):D133–D143.
- 855 Ge, J., Yu, G., Ator, M. A., and Stubbe, J. (2003). Pre-Steady-State and Steady-State Kinetic Analysis of *E. coli* Class
 856 I Ribonucleotide Reductase. *Biochemistry*, 42(34):10071–10083.
- 857 Godin, M., Delgado, F. F., Son, S., Grover, W. H., Bryan, A. K., Tzur, A., Jorgensen, P., Payer, K., Grossman, A. D.,
 858 Kirschner, M. W., and Manalis, S. R. (2010). Using buoyant mass to measure the growth of single cells. *Nature
 859 Methods*, 7(5):387–390.
- 860 Goldman, S. R., Nair, N. U., Wells, C. D., Nickels, B. E., and Hochschild, A. (2015). The primary σ factor in *Es-
 861 cherichia coli* can access the transcription elongation complex from solution *in vivo*. *eLife*, 4:e10514.
- 862 Harris, L. K. and Theriot, J. A. (2018). Surface Area to Volume Ratio: A Natural Variable for Bacterial Morphogen-
 863 esis. *Trends in microbiology*, 26(10):815–832.
- 864 Harris, R. M., Webb, D. C., Howitt, S. M., and Cox, G. B. (2001). Characterization of PitA and PitB from *Escherichia
 865 coli*. *Journal of Bacteriology*, 183(17):5008–5014.
- 866 Heldal, M., Norland, S., and Tumyr, O. (1985). X-ray microanalytic method for measurement of dry matter and
 867 elemental content of individual bacteria. *Applied and Environmental Microbiology*, 50(5):1251–1257.
- 868 Henkel, S. G., Beek, A. T., Steinsiek, S., Stagge, S., Bettenbrock, K., de Mattos, M. J. T., Sauter, T., Sawodny, O.,
 869 and Ederer, M. (2014). Basic Regulatory Principles of *Escherichia coli*'s Electron Transport Chain for Varying
 870 Oxygen Conditions. *PLoS ONE*, 9(9):e107640.
- 871 Ingledew, W. J. and Poole, R. K. (1984). The respiratory chains of *Escherichia coli*. *Microbiological Reviews*,
 872 48(3):222–271.
- 873 Ireland, W. T., Beeler, S. M., Flores-Bautista, E., Belliveau, N. M., Sweredoski, M. J., Moradian, A., Kinney, J. B.,
 874 and Phillips, R. (2020). Deciphering the regulatory genome of *Escherichia coli*, one hundred promoters at a
 875 time. *bioRxiv*.
- 876 Jacob, F. and Monod, J. (1961). Genetic regulatory mechanisms in the synthesis of proteins. *Journal of Molecular
 877 Biology*, 3(3):318–356.
- 878 Jensen, R. B., Wang, S. C., and Shapiro, L. (2001). A moving DNA replication factory in *Caulobacter crescentus*.
 879 *The EMBO journal*, 20(17):4952–4963.
- 880 JL, R., S, V., D, S., ÁD, O., A, S., and M, H. (2016). Bacterial Persistence Is an Active σ S Stress Response to Metabolic
 881 Flux Limitation. *Molecular Systems Biology*, 12(9):882.
- 882 Jun, S., Si, F., Pugatch, R., and Scott, M. (2018). Fundamental principles in bacterial physiology - history, recent
 883 progress, and the future with focus on cell size control: A review. *Reports on Progress in Physics*, 81(5):056601.
- 884 Kapanidis, A. N., Margeat, E., Laurence, T. A., Doose, S., Ho, S. O., Mukhopadhyay, J., Kortkhonjia, E., Mekler, V.,
 885 Ebright, R. H., and Weiss, S. (2005). Retention of Transcription Initiation Factor Σ 70 in Transcription Elonga-
 886 tion: Single-Molecule Analysis. *Molecular Cell*, 20(3):347–356.
- 887 Khademi, S., O'Connell, J., Remis, J., Robles-Colmenares, Y., Miercke, L.J. W., and Stroud, R. M. (2004). Mechanism
 888 of Ammonia Transport by Amt/MEP/Rh: Structure of AmtB at 1.35 Å. *Science*, 305(5690):1587–1594.

- 889 Khademian, M. and Imlay, J. A. (2017). *Escherichia coli* cytochrome c peroxidase is a respiratory oxidase that
890 enables the use of hydrogen peroxide as a terminal electron acceptor. *Proceedings of the National Academy
891 of Sciences*, 114(33):E6922–E6931.
- 892 Li, G.-W., Burkhardt, D., Gross, C., and Weissman, J. S. (2014). Quantifying absolute protein synthesis rates
893 reveals principles underlying allocation of cellular resources. *Cell*, 157(3):624–635.
- 894 Liu, M., Durfee, T., Cabrera, J. E., Zhao, K., Jin, D. J., and Blattner, F. R. (2005). Global Transcriptional Programs
895 Reveal a Carbon Source Foraging Strategy by *Escherichia coli*. *Journal of Biological Chemistry*, 280(16):15921–
896 15927.
- 897 Lu, D., Grayson, P., and Schulten, K. (2003). Glycerol Conductance and Physical Asymmetry of the *Escherichia
898 coli* Glycerol Facilitator GlpF. *Biophysical Journal*, 85(5):2977–2987.
- 899 Lynch, M. and Marinov, G. K. (2015). The bioenergetic costs of a gene. *Proceedings of the National Academy of
900 Sciences*, 112(51):15690–15695.
- 901 Maaløe, O. (1979). *Regulation of the Protein-Synthesizing Machinery—Ribosomes, tRNA, Factors, and So On. Gene
902 Expression*. Springer.
- 903 Milo, R., Jorgensen, P., Moran, U., Weber, G., and Springer, M. (2010). BioNumbers—the database of key num-
904 bers in molecular and cell biology. *Nucleic Acids Research*, 38(suppl_1):D750–D753.
- 905 Monod, J. (1947). The phenomenon of enzymatic adaptation and its bearings on problems of genetics and
906 cellular differentiation. *Growth Symposium*, 9:223–289.
- 907 Mooney, R. A., Darst, S. A., and Landick, R. (2005). Sigma and RNA Polymerase: An On-Again, Off-Again Rela-
908 tionship? *Molecular Cell*, 20(3):335–345.
- 909 Mooney, R. A. and Landick, R. (2003). Tethering Σ 70 to RNA polymerase reveals high *in vivo* activity of σ factors
910 and Σ 70-dependent pausing at promoter-distal locations. *Genes & Development*, 17(22):2839–2851.
- 911 Neidhardt, F. C., Ingraham, J., and Schaechter, M. (1991). *Physiology of the Bacterial Cell - A Molecular Approach*,
912 volume 1. Elsevier.
- 913 Ojkic, N., Serbanescu, D., and Banerjee, S. (2019). Surface-to-volume scaling and aspect ratio preservation in
914 rod-shaped bacteria. *eLife*, 8:642.
- 915 Patrick, M., Dennis, P. P., Ehrenberg, M., and Bremer, H. (2015). Free RNA polymerase in *Escherichia coli*.
916 *Biochimie*, 119:80–91.
- 917 Peebo, K., Valgepea, K., Maser, A., Nahku, R., Adamberg, K., and Vilu, R. (2015). Proteome reallocation in *Es-
918 cherichia coli* with increasing specific growth rate. *Molecular BioSystems*, 11(4):1184–1193.
- 919 Perdue, S. A. and Roberts, J. W. (2011). σ^{70} -dependent Transcription Pausing in *Escherichia coli*. *Journal of
920 Molecular Biology*, 412(5):782–792.
- 921 Phillips, R. (2018). Membranes by the Numbers. In *Physics of Biological Membranes*, pages 73–105. Springer,
922 Cham, Cham.
- 923 Ramos, S. and Kaback, H. R. (1977). The relation between the electrochemical proton gradient and active trans-
924 port in *Escherichia coli* membrane vesicles. *Biochemistry*, 16(5):854–859.
- 925 Rosenberg, H., Gerdes, R. G., and Chegwidden, K. (1977). Two systems for the uptake of phosphate in *Escherichia
926 coli*. *Journal of Bacteriology*, 131(2):505–511.
- 927 Rudd, S. G., Valerie, N. C. K., and Helleday, T. (2016). Pathways controlling dNTP pools to maintain genome
928 stability. *DNA Repair*, 44:193–204.
- 929 Sánchez-Romero, M. A., Molina, F., and Jiménez-Sánchez, A. (2011). Organization of ribonucleoside diphosphate
930 reductase during multifork chromosome replication in *Escherichia coli*. *Microbiology*, 157(8):2220–2225.
- 931 Schaechter, M., Maaløe, O., and Kjeldgaard, N. O. (1958). Dependency on Medium and Temperature of Cell Size
932 and Chemical Composition during Balanced Growth of *Salmonella typhimurium*. *Microbiology*, 19(3):592–606.
- 933 Schmidt, A., Kochanowski, K., Vedelaar, S., Ahrné, E., Volkmer, B., Callipo, L., Knoops, K., Bauer, M., Aebersold,
934 R., and Heinemann, M. (2016). The quantitative and condition-dependent *Escherichia coli* proteome. *Nature
935 Biotechnology*, 34(1):104–110.

- 936 Scholz, S. A., Diao, R., Wolfe, M. B., Fivenson, E. M., Lin, X. N., and Freddolino, P. L. (2019). High-Resolution
 937 Mapping of the *Escherichia coli* Chromosome Reveals Positions of High and Low Transcription. *Cell Systems*,
 938 8(3):212–225.e9.
- 939 Scott, M., Gunderson, C. W., Mateescu, E. M., Zhang, Z., and Hwa, T. (2010). Interdependence of cell growth and
 940 gene expression: origins and consequences. *Science*, 330(6007):1099–1102.
- 941 Sekowska, A., Kung, H.-F., and Danchin, A. (2000). Sulfur Metabolism in *Escherichia coli* and Related Bacteria:
 942 Facts and Fiction. *Journal of Molecular Microbiology and Biotechnology*, 2(2):34.
- 943 Shi, H., Bratton, B. P., Gitai, Z., and Huang, K. C. (2018). How to Build a Bacterial Cell: MreB as the Foreman of
 944 *E. coli* Construction. *Cell*, 172(6):1294–1305.
- 945 Si, F., Le Treut, G., Sauls, J. T., Vadia, S., Levin, P. A., and Jun, S. (2019). Mechanistic Origin of Cell-Size Control
 946 and Homeostasis in Bacteria. *Current Biology*, 29(11):1760–1770.e7.
- 947 Si, F., Li, D., Cox, S. E., Sauls, J. T., Azizi, O., Sou, C., Schwartz, A. B., Erickstad, M. J., Jun, Y., Li, X., and Jun, S. (2017).
 948 Invariance of Initiation Mass and Predictability of Cell Size in *Escherichia coli*. *Current Biology*, 27(9):1278–1287.
- 949 Sirko, A., Zatyka, M., Sadowy, E., and Hulanicka, D. (1995). Sulfate and thiosulfate transport in *Escherichia coli* K-
 950 12: Evidence for a functional overlapping of sulfate- and thiosulfate-binding proteins. *Journal of Bacteriology*,
 951 177(14):4134–4136.
- 952 Stasi, R., Neves, H. I., and Spira, B. (2019). Phosphate uptake by the phosphonate transport system PhnCDE.
 953 *BMC Microbiology*, 19.
- 954 Stevenson, B. S. and Schmidt, T. M. (2004). Life History Implications of rRNA Gene Copy Number in *Escherichia coli*.
 955 *Applied and Environmental Microbiology*, 70(11):6670–6677.
- 956 Stouthamer, A. H. (1973). A theoretical study on the amount of ATP required for synthesis of microbial cell
 957 material. *Antonie van Leeuwenhoek*, 39(1):545–565.
- 958 Stouthamer, A. H. and Bettenhausen, C. W. (1977). A continuous culture study of an ATPase-negative mutant
 959 of *Escherichia coli*. *Archives of Microbiology*, 113(3):185–189.
- 960 Svenningsen, S. L., Kongstad, M., Stenum, T. S. n., Muñoz-Gómez, A. J., and Sørensen, M. A. (2017). Transfer RNA
 961 is highly unstable during early amino acid starvation in *Escherichia coli*. *Nucleic Acids Research*, 45(2):793–804.
- 962 Szenk, M., Dill, K. A., and de Graff, A. M. R. (2017). Why Do Fast-Growing Bacteria Enter Overflow Metabolism?
 963 Testing the Membrane Real Estate Hypothesis. *Cell Systems*, 5(2):95–104.
- 964 Taheri-Araghi, S., Bradde, S., Sauls, J. T., Hill, N. S., Levin, P. A., Paulsson, J., Vergassola, M., and Jun, S. (2015).
 965 Cell-size control and homeostasis in bacteria. - PubMed - NCBI. *Current Biology*, 25(3):385–391.
- 966 Tatusov, R. L., Galperin, M. Y., Natale, D. A., and Koonin, E. V. (2000). The COG database: a tool for genome-scale
 967 analysis of protein functions and evolution. *Nucleic Acids Research*, 28(1):33–36.
- 968 Taymaz-Nikerel, H., Borujeni, A. E., Verheijen, P. J. T., Heijnen, J. J., and van Gulik, W. M. (2010).
 969 Genome-derived minimal metabolic models for *Escherichia coli* mg1655 with estimated in vivo
 970 respiratory ATP stoichiometry. *Biotechnology and Bioengineering*, 107(2):369–381. _eprint:
 971 <https://onlinelibrary.wiley.com/doi/pdf/10.1002/bit.22802>.
- 972 The Gene Ontology Consortium (2018). The Gene Ontology Resource: 20 years and still GOing strong. *Nucleic
 973 Acids Research*, 47(D1):D330–D338.
- 974 Valgepea, K., Adamberg, K., Seiman, A., and Vilu, R. (2013). *Escherichia coli* achieves faster growth by increasing
 975 catalytic and translation rates of proteins. *Molecular BioSystems*, 9(9):2344.
- 976 van Heeswijk, W. C., Westerhoff, H. V., and Boogerd, F. C. (2013). Nitrogen Assimilation in *Escherichia coli*: Putting
 977 Molecular Data into a Systems Perspective. *Microbiology and Molecular Biology Reviews*, 77(4):628–695.
- 978 Weber, J. and Senior, A. E. (2003). ATP synthesis driven by proton transport in F1FO-ATP synthase. *FEBS Letters*,
 979 545(1):61–70.
- 980 Willsky, G. R., Bennett, R. L., and Malamy, M. H. (1973). Inorganic Phosphate Transport in *Escherichia coli*: Involvement
 981 of Two Genes Which Play a Role in Alkaline Phosphatase Regulation. *Journal of Bacteriology*, 113(2):529–
 982 539.

- 983 Zhang, L., Jiang, W., Nan, J., Almqvist, J., and Huang, Y. (2014a). The *Escherichia coli* CysZ is a pH dependent sulfate
984 transporter that can be inhibited by sulfite. *Biochimica et Biophysica Acta (BBA) - Biomembranes*, 1838(7):1809–
985 1816.
- 986 Zhang, Z., Aboulwafa, M., and Saier, M. H. (2014b). Regulation of crp gene expression by the catabolite repres-
987 sor/activator, cra, in *Escherichia coli*. *Journal of Molecular Microbiology and Biotechnology*, 24(3):135–141.
- 988 Zhu, M. and Dai, X. (2019). Growth suppression by altered (p)ppGpp levels results from non-optimal resource
989 allocation in *Escherichia coli*. *Nucleic Acids Research*, 47(9):4684–4693.